SIAM J. SCI. COMPUT.
Vol. 41, No. 2, pp. A1121–A1147

ROBUST ADAPTIVE *hp* DISCONTINUOUS GALERKIN FINITE ELEMENT METHODS FOR THE HELMHOLTZ EQUATION*

SCOTT CONGREVE†, JOSCHA GEDICKE†, AND ILARIA PERUGIA†

Abstract. This paper presents an *hp* a posteriori error analysis for the 2D Helmholtz equation that is robust in the polynomial degree p and the wave number k. For the discretization, we consider a discontinuous Galerkin formulation that is unconditionally well posed. The a posteriori error analysis is based on the technique of equilibrated fluxes applied to a shifted Poisson problem, with the error due to the nonconformity of the discretization controlled by a potential reconstruction. We prove that the error estimator is both reliable and efficient, under the condition that the initial mesh size and polynomial degree are chosen such that the discontinuous Galerkin formulation converges, i.e., it is out of the regime of pollution. We confirm the efficiency of an *hp*-adaptive refinement strategy based on the presented robust a posteriori error estimator via several numerical examples.

Key words. a posteriori error analysis, *hp* discontinuous Galerkin finite element method, equilibrated fluxes, potential reconstruction, Helmholtz problem

AMS subject classifications. 65N15, 65N30, 65N50

DOI. 10.1137/18M1207909

1. Introduction.

In this paper, we consider the following Helmholtz problem with an impedance boundary condition: Find a (complex) solution $u \in H^2(\Omega)$ such that

$$\begin{aligned} -\Delta u - k^2 u &= f \quad \text{in } \Omega, \\ \nabla u \cdot \boldsymbol{n} - iku &= g \quad \text{on } \partial\Omega, \end{aligned} \tag{1.1}$$

where $\Omega \subset \mathbb{R}^2$ is a bounded, Lipschitz domain, $\boldsymbol{n}$ denotes the outer unit normal on the boundary $\partial\Omega$, $f \in L^2(\Omega)$, $g \in L^2(\partial\Omega)$, and $k > 0$ is the (constant) wave number.

The problem (1.1) was shown to be well posed in [18]. A polynomial-based discontinuous Galerkin (DG) approximation was presented in [19], which uses the same numerical fluxes as in the ultra weak variational formulation/plane wave DG methods [9, 10, 15]. A DG discretization with stabilization terms also containing jumps in high-order derivatives was presented in [14]. A residual-based a posteriori error estimator for the DG method of [19] is derived and analyzed in [23].

In this paper, we will develop an a posteriori error estimator based on a local reconstruction of equilibrated fluxes [11, 12]. Since (1.1) is highly indefinite, it is not clear how to localize the Helmholtz problem in order to obtain localized problems for the error approximation that are well posed. However, as noted in [1], the error has two components, the interpolation error and the pollution error. While the pollution error is global and hence cannot be estimated with local error indicators, it is possible to derive equilibrated a posteriori error estimators for the interpolation error.

*Submitted to the journal's Methods and Algorithms for Scientific Computing section August 16, 2018; accepted for publication (in revised form) January 29, 2019; published electronically April 11, 2019.

http://www.siam.org/journals/sisc/41-2/M120790.html

Funding: This work was supported by the Austrian Science Fund (FWF) through projects F 65 and P 29197-N32 and by the Vienna Science and Technology Fund (WWTF) through the project MA14-006.

†Faculty of Mathematics, University of Vienna, 1090 Vienna, Austria (scott.congreve@univie.ac.at, joscha.gedicke@univie.ac.at, ilaria.perugia@univie.ac.at).

This analysis is based on considering a shifted Poisson problem with inhomogeneous Neumann boundary conditions. Therefore, we can apply the unified framework for equilibrated fluxes [12] to this auxiliary elliptic problem with an extension for the extra terms resulting from the handling of the inhomogeneous Robin boundary condition by the DG method. Additionally, an extra lifting operator is required due to the additional gradient stabilization terms in the DG formulation for Helmholtz. In order to measure the nonconformity of the DG method, we locally reconstruct a conforming potential approximation.

By construction, the a posteriori error estimator captures possible singularities of the solution correctly, but is only reliable up to an additional L^2 error which resembles the pollution error. Note that also the residual a posteriori error estimator for the DG method in [23] is only reliable up to the pollution error; see [23, Lemma 3.2].

We will apply the theory of equilibrated flux and potential reconstructions [11, 12] and derive the a posteriori error estimator of the form

$$\begin{aligned}\eta_{hp}^2 := \sum_{T\in\mathcal{T}} \Bigg(& \|\mathcal{G}(u_{hp}) + \boldsymbol{\sigma}_{hp}\|_{0,T} + \frac{h_T}{j_{1,1}}\|f + k^2 u_{hp} - \operatorname{div}\boldsymbol{\sigma}_{hp}\|_{0,T} \\ & + C_{tr} \sum_{E\in\mathcal{E}(T)\cap\mathcal{E}(\partial\Omega)} h_E^{1/2} \|\boldsymbol{\sigma}_{hp}\cdot\boldsymbol{n} + g + iku_{hp} - \gamma k \frac{\mathsf{h}}{\mathsf{p}}(g - \nabla_h u_{hp}\cdot\boldsymbol{n} + iku_{hp})\|_{0,E} \Bigg)^2 \\ & + \sum_{T\in\mathcal{T}} \|\mathcal{G}(u_{hp}) - \nabla s_{hp}\|_{0,T}^2,\end{aligned}$$

where $\mathcal{G}(u_{hp})$ denotes a discrete gradient (which we call the *DG gradient*), $\boldsymbol{\sigma}_{hp}$ an equilibrated flux reconstruction, and s_{hp} a potential reconstruction. The parameter γ, as well as the mesh function h and the polynomial degree function p, already enter the definition of the DG methods (see (2.3) below), h_T and h_E are the diameter of the element T of the mesh $\mathcal{T}$ and the edge E of T, respectively, C_{tr} is a trace inequality constant (cf. Lemma 3.4), and $j_{1,1}$ is the first positive root of the Bessel function of the first kind. We prove that the a posteriori error estimator is reliable and efficient, for suitably chosen functions $\boldsymbol{\sigma}_{hp}$ and s_{hp}, up to generic constants which are independent of the wave number, the polynomial degrees, and the element sizes.

This paper is organized as follows. In section 2, we will recall the DG method from [19]. In section 3, we will present the a posteriori error estimator and prove its reliability for any admissible flux and potential reconstructions. In section 4, we define specific local reconstructions of flux and potential functions, such that the error estimator is efficient. Finally, in section 5, we present some numerical experiments.

Throughout this paper, we employ the standard notation for (complex) Sobolev spaces $H^m(\omega)$ with norm $\|\cdot\|_{m,\omega}$ for (sub-)domains $\omega \subseteq \Omega$ and define $H(\operatorname{div};\Omega) = \{\boldsymbol{\tau} \in [L^2(\omega)]^2 : \operatorname{div}\boldsymbol{\tau} \in L^2(\omega)\}$. We denote the (complex) L^2 inner product by $(\cdot,\cdot)_\omega$; if $\omega = \Omega$, we simply write $(\cdot,\cdot)$. The (complex) L^2 inner product on the boundary is indicated by a subscript, e.g., $(\cdot,\cdot)_{\partial\omega}$. By $\lesssim$, we abbreviate the inequality $x \le Cy$, with a generic constant C independent of the wave number, the mesh size, and the polynomial degree, but possibly dependent on the shape regularity of the mesh.

2. The discontinuous Galerkin method. In this section, we discuss a numerical approximation to (1.1) based on employing an *hp*-version DG finite element method. We consider the same formulation as in [19].

The weak formulation of (1.1) is defined as follows: Find $u \in H^1(\Omega)$ such that

$$a(u,v) = F(v) \quad \text{for all } v \in H^1(\Omega), \tag{2.1}$$

with the complex-valued sesquilinear form $a(\cdot,\cdot)$ and linear form $F(\cdot)$ given by

$$a(u,v) := (\nabla u, \nabla v) - k^2(u,v) - ik(u,v)_{\partial\Omega} \quad \text{and} \quad F(v) := (f,v) + (g,v)_{\partial\Omega}.$$

Let $\mathcal{T}$ be a triangulation of Ω with the set of nodes $\mathcal{N}$ and the set of edges $\mathcal{E}$. For simplicity of the presentation, we restrict ourselves to shape-regular conforming triangulations. Let $\mathcal{E}(\Omega)$ and $\mathcal{E}(\partial\Omega)$ denote the subset of interior and boundary edges, respectively, and let $\mathcal{E}(T)$ denote the edges of the element $T \in \mathcal{T}$. Let $\mathcal{N}(\partial\Omega)$ denote the subset of nodes on the boundary of Ω, $\mathcal{N}(T)$ denote the set of nodes of an element $T \in \mathcal{T}$, and $\mathcal{N}(E)$ denote the set of nodes of an edge $E \in \mathcal{E}$. The subset of triangles that share a common node $z \in \mathcal{N}$ is denoted by $\mathcal{T}(z)$, and the subset of edges sharing the node z is denoted by $\mathcal{E}(z)$. For any node $z \in \mathcal{N}$, we denote by $\omega_z \subseteq \Omega$ the union of triangles that share the node z. The set of triangles that share a common edge $E \in \mathcal{E}(\Omega)$ is denoted by $\mathcal{T}(E)$. For any $E \in \mathcal{E}(\Omega)$, we denote by $\omega_E \subseteq \Omega$ the union of the two triangles $T_\pm \in \mathcal{T}$ that share the edge E; we set $\omega_E = T$ for $E \in \mathcal{E}(\partial\Omega)$. We denote by h_T and h_E the diameter of T and the length of E, respectively.

We make use of the standard notation on averages and jumps of scalar functions v across edges $E \in \mathcal{E}(\Omega)$ with $E = \partial T_+ \cap \partial T_-$:

$$\{\!\{v\}\!\} := \frac{1}{2}\left(v|_{T_+} + v|_{T_-}\right), \qquad [\![v]\!]_N := v|_{T_+}\boldsymbol{n}_+ + v|_{T_-}\boldsymbol{n}_- \tag{2.2}$$

and, for vector-valued functions $\boldsymbol{\tau}$,

$$\{\!\{\boldsymbol{\tau}\}\!\} := \frac{1}{2}\left(\boldsymbol{\tau}|_{T_+} + \boldsymbol{\tau}|_{T_-}\right), \qquad [\![\boldsymbol{\tau}]\!]_N := \boldsymbol{\tau}|_{T_+}\cdot\boldsymbol{n}_+ + \boldsymbol{\tau}|_{T_-}\cdot\boldsymbol{n}_-,$$

where $\boldsymbol{n}_\pm$ denotes the unit outer normal vector of $T_\pm$. For any scalar function $v = v(x_1,x_2)$, we denote by $\mathbf{rot}\, v = [\frac{\partial v}{\partial x_2}, -\frac{\partial v}{\partial x_1}]^\top$ the *rotation* of v, and we denote the elementwise application of the gradient and rotation by ∇_h and $\mathbf{rot}_h$, respectively, i.e., $(\nabla_h \cdot)|_T = \nabla(\cdot)|_T$ and $(\mathbf{rot}_h\, \cdot)|_T = \mathbf{rot}(\cdot)|_T$ for all $T \in \mathcal{T}$.

Let V_{hp} denote the discontinuous finite element space of piecewise polynomial basis functions

$$V_{hp} := \{v_{hp} \in L^2(\Omega) \,:\, v_{hp}|_T \in \mathbb{P}_{p_T}(T) \text{ for all } T \in \mathcal{T}\},$$

where $\mathbb{P}_{p_T}(T)$ denotes the space of polynomials of degree less than or equal to $p_T \geq 1$ on a triangle $T \in \mathcal{T}$. Let us denote by h and p the piecewise constant mesh size function and polynomial degree function, respectively, defined on the mesh interfaces as follows: $\mathsf{h}|_E = \min(h_{T_+}, h_{T_-})$ and $\mathsf{p}|_E = \max(p_{T_+}, p_{T_-})$ if $E = \partial T_+ \cap \partial T_-$, or $\mathsf{h}|_E = h_T$ and $\mathsf{p}|_E = p_T$ if $E \subseteq \partial T \cap \partial\Omega$.

The discrete problem then reads as follows: Find $u_{hp} \in V_{hp}$ such that

$$a_{hp}(u_{hp}, v_{hp}) = F_{hp}(v_{hp}) \quad \text{for all } v_{hp} \in V_{hp}, \tag{2.3}$$

where

$$\begin{aligned} a_{hp}(u,v) := {} & (\nabla_h u, \nabla_h v) - k^2(u,v) \\ & - \sum_{E\in\mathcal{E}(\Omega)} ([\![u]\!]_N, \{\!\{\nabla_h v\}\!\})_E - \sum_{E\in\mathcal{E}(\Omega)} (\{\!\{\nabla_h u\}\!\}, [\![v]\!]_N)_E \\ & - \left(\gamma k \frac{\mathsf{h}}{\mathsf{p}} u, \nabla_h v\cdot\boldsymbol{n}\right)_{\partial\Omega} - \left(\gamma k \frac{\mathsf{h}}{\mathsf{p}} \nabla_h u\cdot\boldsymbol{n}, v\right)_{\partial\Omega} \end{aligned}$$

$$- i \sum_{E\in\mathcal{E}(\Omega)} \left(\beta\frac{\mathsf{h}}{\mathsf{p}}[\![\nabla_h u]\!]_N, [\![\nabla_h v]\!]_N\right)_E - i \sum_{E\in\mathcal{E}(\Omega)} \left(\alpha\frac{\mathsf{p}^2}{\mathsf{h}}[\![u]\!]_N, [\![v]\!]_N\right)_E$$
$$- i\left(\gamma\frac{\mathsf{h}}{\mathsf{p}}\nabla_h u\cdot\boldsymbol{n}, \nabla_h v\cdot\boldsymbol{n}\right)_{\partial\Omega} - i\left(k(1-\gamma k\frac{\mathsf{h}}{\mathsf{p}})u, v\right)_{\partial\Omega}$$

and

$$F_{hp}(v) := (f,v) - i\left(\frac{\gamma\mathsf{h}}{\mathsf{p}}g, \nabla_h v\cdot\boldsymbol{n}\right)_{\partial\Omega} + \left((1-\gamma k\frac{\mathsf{h}}{\mathsf{p}})g, v\right)_{\partial\Omega}.$$

The constants $\alpha > 0$, $\beta > 0$, and $0 < \gamma < 1/3$ are fixed constants. Note that $\beta > 0$ guarantees the unconditional well posedness of the discrete problem; cf. [19].

In order to define the DG gradient (see Definition 2.2 below), we need to introduce two lifting operators. For any $E \in \mathcal{E}(\Omega)$, let

$$\mathbb{P}_0(\mathcal{T}(E))^2 := \{v_{hp} \in [L^2(\omega_E)]^2 \,:\, v_{hp}|_T \in [\mathbb{P}_0(T)]^2 \text{ for all } T \in \mathcal{T}(E)\};$$

then, we define $\mathcal{L}_E^0 \in \mathbb{P}_0(\mathcal{T}(E))^2$ as

$$\int_{\omega_E} \mathcal{L}_E^0([\![v_{hp}]\!]_N)\cdot\overline{\boldsymbol{\tau}}_{hp}\,dx = \int_E [\![v_{hp}]\!]_N \cdot \{\!\{\overline{\boldsymbol{\tau}}_{hp}\}\!\}\,ds$$

for all $\boldsymbol{\tau}_{hp} \in \mathbb{P}_0(\mathcal{T}(E))^2$, and we define $\mathcal{L}_E^1 \in \mathbb{P}_0(\mathcal{T}(E))^2$ as

$$\int_{\omega_E} \mathcal{L}_E^1([\![\nabla_h v_{hp}]\!]_N)\cdot\overline{\boldsymbol{\tau}}_{hp}\,dx = i\beta\int_E \frac{\mathsf{h}}{\mathsf{p}}[\![\nabla_h v_{hp}]\!]_N[\![\overline{\boldsymbol{\tau}}_{hp}]\!]_N\,ds$$

for all $\boldsymbol{\tau}_{hp} \in \mathbb{P}_0(\mathcal{T}(E))^2$.

For a given integer $p \geq 0$, let $\Pi_E^p : L^2(E) \to \mathbb{P}_p(E)$ denote the local L^2-orthogonal projection onto the space of polynomials of degree at most p along the edge $E \in \mathcal{E}$. Similarly, we define $\Pi_T^p : L^2(T) \to \mathbb{P}_p(T)$ to be the local L^2-orthogonal projection onto the space of polynomials of degree at most p on a triangle $T \in \mathcal{T}$.

We can derive the following stability estimates following along the lines of the proof of [21, Proposition 4.2].

LEMMA 2.1. *The lifting operators $\mathcal{L}_E^0$ and $\mathcal{L}_E^1$ are stable in the sense that*

$$\|\mathcal{L}_E^0([\![v_{hp}]\!]_N)\|_{0,T} \lesssim h_E^{-1/2}\|\Pi_E^0([\![v_{hp}]\!]_N)\|_{0,E},$$
$$\|\mathcal{L}_E^1([\![\nabla v_{hp}]\!]_N)\|_{0,T} \lesssim \beta h_E^{1/2}\|\mathsf{p}^{-1}\Pi_E^0([\![\nabla v_{hp}]\!]_N)\|_{0,E}$$

for $T = T_\pm$, where $T_\pm$ are the two elements sharing the edge E.

Proof. For any $\boldsymbol{\tau}_{hp} \in \mathbb{P}_0(\mathcal{T}(E))^2$, we have that $h_E^{-1}\|\boldsymbol{\tau}_{hp}\|_{0,E}^2 = |T|^{-1}\|\boldsymbol{\tau}_{hp}\|_{0,T}^2$, $T = T_\pm$. Hence,

$$\begin{aligned}
\|\mathcal{L}_E^0([\![v_{hp}]\!]_N)\|_{0,T} &\leq \|\mathcal{L}_E^0([\![v_{hp}]\!]_N)\|_{0,\omega_E}\\
&= \sup_{\boldsymbol{\tau}_{hp}\in\mathbb{P}_0(\mathcal{T}(E))^2,\,\|\boldsymbol{\tau}_{hp}\|_{0,\omega_E}=1} \int_{\omega_E} \mathcal{L}_E^0([\![v_{hp}]\!]_N)\cdot\overline{\boldsymbol{\tau}}_{hp}\,dx\\
&= \sup_{\boldsymbol{\tau}_{hp}\in\mathbb{P}_0(\mathcal{T}(E))^2,\,\|\boldsymbol{\tau}_{hp}\|_{0,\omega_E}=1} \int_E \Pi_E^0([\![v_{hp}]\!]_N)\cdot\{\!\{\overline{\boldsymbol{\tau}}_{hp}\}\!\}\,ds\\
&\leq Ch_E^{-1/2}\|\Pi_E^0([\![v_{hp}]\!]_N)\|_{0,E},
\end{aligned}$$

where $C = h_E\max\{|T_+|^{-1/2}, |T_-|^{-1/2}\}$ is bounded by shape regularity. The second bound follows similarly. ∎

DEFINITION 2.2 (DG gradient). *We define the DG gradient by*

$$\mathcal{G}(u_{hp}) := \nabla_h u_{hp} - \sum_{E\in\mathcal{E}(\Omega)} \mathcal{L}_E^0([\![u_{hp}]\!]_N) - \sum_{E\in\mathcal{E}(\Omega)} \mathcal{L}_E^1([\![\nabla u_{hp}]\!]_N). \tag{2.4}$$

Remark 2.3. The lifting operators $\mathcal{L}_E^0$ arise already in [12] for the DG discretization of the Poisson problem, whereas the lifting operators $\mathcal{L}_E^1$ are required due to the additional gradient stabilization terms in the formulation (2.3).

3. A posteriori error estimator and reliability. In this section, we derive an equilibrated a posteriori error estimator based on a shifted Poisson problem and prove that it is reliable, up to additional L^2 and boundary errors. The definition of this estimator involves flux and potential reconstructions, which will be defined below. This approach is also related to the a posteriori error analysis for the eigenvalue problem via equilibrated fluxes developed in [5, 6].

For simplicity of the presentation of the equilibrated flux technique, we restrict ourselves to conforming meshes with no hanging nodes. For the necessary modifications to handle irregular meshes we refer the reader to [11].

We approach the a posteriori error estimation of the DG finite element approximation of the Helmholtz problem by considering the following (shifted) Poisson problem with Neumann boundary conditions: Find a (complex) function $w \in H^2(\Omega)$ such that

$$\begin{aligned} -\Delta w &= f + k^2 u_{hp} && \text{in } \Omega, \\ \nabla w \cdot \boldsymbol{n} &= g + iku_{hp} - \gamma k \frac{\mathsf{h}}{\mathsf{p}}(g - \nabla_h u_{hp}\cdot\boldsymbol{n} + iku_{hp}) && \text{on } \partial\Omega. \end{aligned} \tag{3.1}$$

Note that the boundary condition is chosen in such a way that the compatibility condition for the pure Neumann problem is satisfied due to (2.3).

DEFINITION 3.1 (flux reconstruction). *For a given $u_{hp} \in V_{hp}$, we define an* equilibrated flux reconstruction *for u_{hp} as any function $\boldsymbol{\sigma}_{hp} \in H(\mathrm{div};\Omega)$ which satisfies*

$$\begin{aligned} \int_T \mathrm{div}\,\boldsymbol{\sigma}_{hp}\,dx &= \int_T f + k^2 u_{hp}\,dx && \text{for all } T\in\mathcal{T}, \\ \int_E \boldsymbol{\sigma}_{hp}\cdot\boldsymbol{n}\,ds &= \int_E -(g+iku_{hp}) + \gamma k\frac{\mathsf{h}}{\mathsf{p}}(g - \nabla_h u_{hp}\cdot\boldsymbol{n} - iku_{hp})\,ds && \text{for all } E\in\mathcal{E}(\partial\Omega). \end{aligned} \tag{3.2}$$

Since the compatibility condition of the pure Neumann problem is satisfied, the existence of such a function follows from the mixed theory applied to the homogeneous Neumann problem in $H_0(\mathrm{div};\Omega)\times L_0^2(\Omega)$, where

$$H_0(\mathrm{div};\Omega) := \{\tau \in H(\mathrm{div};\Omega) \,:\, \tau\cdot\boldsymbol{n} = 0 \text{ on } \partial\Omega\},$$
$$L_0^2(\Omega) := \left\{ v\in L^2(\Omega) \,:\, \int_\Omega v\,dx = 0\right\}.$$

By proceeding as in the Dirichlet case [3, Example 4.2.1], this relies on the surjectivity of $\mathrm{div} : H_0(\mathrm{div};\Omega) \to L_0^2(\Omega)$ (see, e.g., [3, equation (4.2.62)]).

We point out that $\boldsymbol{\sigma}_{hp}$ is not necessarily a piecewise polynomial function; the subscript hp simply indicates that it is associated with a piecewise polynomial function (namely u_{hp}).

DEFINITION 3.2 (potential). *We define a* potential *as any function*

$$s_{hp} \in H_*^1(\Omega) := \{v\in H^1(\Omega) \,:\, (v,1) = 0\}.$$

As for $\boldsymbol{\sigma}_{hp}$, the subscript hp indicates that s_{hp} will be constructed from u_{hp}; see section 4.2 below. For this reason, we will call s_{hp} a *potential reconstruction* for u_{hp}.

For the proof of reliability of the error estimator (see (3.4) below), the following Poincaré and trace estimates, with explicit constants for triangles, are required.

LEMMA 3.3 (Poincaré inequality on triangles [17]). *For any $v \in H^1(T)$, where T is a triangle, it holds that*

$$\|v - \Pi_T^0 v\|_{0,T} \leq \frac{h_T}{j_{1,1}} \|\nabla v\|_{0,T}, \tag{3.3}$$

where $j_{1,1} \approx 3.83170597020751$ denotes the first positive root of the Bessel function of the first kind.

LEMMA 3.4. *For any $v \in H^1(T)$, where T is a triangle, we have the following trace estimate for any edge E of T:*

$$h_E^{-1/2} \|v - \Pi_T^0 v\|_{0,E} \leq C_{tr} \|\nabla v\|_{0,T},$$

where $C_{tr}^2 = (j_{1,1}^{-1} + j_{1,1}^{-2}) \frac{h_T^2}{|T|} \leq 0.3291 \frac{h_T^2}{|T|}$.

Proof. The trace identity of [8, Lemma 2.1] leads to the inequality

$$h_E^{-1} \|v - \Pi_T^0 v\|_{0,E}^2 \leq \frac{h_T}{|T|} \|v - \Pi_T^0 v\|_{0,T} \|\nabla v\|_{0,T} + \frac{1}{|T|} \|v - \Pi_T^0 v\|_{0,T}^2.$$

This, together with the Poincaré inequality (3.3), yields

$$h_E^{-1} \|v - \Pi_T^0 v\|_{0,E}^2 \leq \frac{h_T^2}{j_{1,1}|T|} \|\nabla v\|_{0,T}^2 + \frac{h_T^2}{j_{1,1}^2|T|} \|\nabla v\|_{0,T}^2. \qquad \square$$

Remark 3.5. For the adaptive meshes used in section 5, which consist only of right-angled triangles, it holds that $h_T^2/|T| = 4$ and, therefore, $C_{tr} \leq 1.14733$.

We can now define the following error estimator:

$$\begin{aligned} \eta_{hp}^2 := \sum_{T \in \mathcal{T}} \Bigg(& \|\mathcal{G}(u_{hp}) + \boldsymbol{\sigma}_{hp}\|_{0,T} + \frac{h_T}{j_{1,1}} \|f + k^2 u_{hp} - \operatorname{div} \boldsymbol{\sigma}_{hp}\|_{0,T} \\ & + C_{tr} \sum_{E \in \mathcal{E}(T) \cap \mathcal{E}(\partial\Omega)} h_E^{1/2} \|\boldsymbol{\sigma}_{hp} \cdot \boldsymbol{n} + g + iku_{hp} - \gamma k \frac{\mathsf{h}}{\mathsf{p}} (g - \nabla_h u_{hp} \cdot \boldsymbol{n} + iku_{hp})\|_{0,E} \Bigg)^2 \\ & + \sum_{T \in \mathcal{T}} \|\mathcal{G}(u_{hp}) - \nabla s_{hp}\|_{0,T}^2, \end{aligned} \tag{3.4}$$

where $\boldsymbol{\sigma}_{hp} \in H(\operatorname{div}; \Omega)$ is an equilibrated flux reconstruction of u_{hp} as in Definition 3.1, and $s_{hp} \in H_*^1(\Omega)$ is a potential as in Definition 3.2. In the following theorem, we prove the reliability of the estimator defined in (3.4), up to additional L^2 and boundary errors. Notice that we are still in the abstract setting, where $\boldsymbol{\sigma}_{hp}$ and s_{hp} are any admissible flux and potential reconstructions, according to Definitions 3.1 and 3.2, respectively. A specific choice of $\boldsymbol{\sigma}_{hp}$ and s_{hp}, for which efficiency can also be proven, will be given in section 4 below.

THEOREM 3.6 (reliability). *Let $u \in H^1(\Omega)$ be the weak solution of the Helmholtz problem (2.1), and let $u_{hp} \in V_{hp}$ be the discrete solution of (2.3). Then, for the error estimator defined in (3.4), we have that*

$$\begin{aligned}\|\nabla u - \mathcal{G}(u_{hp})\|_{0,\Omega} \lesssim \eta_{hp} + k^2\|u - u_{hp}\|_{0,\Omega} + k\|u - u_{hp}\|_{0,\partial\Omega} \\ + \|\gamma k \frac{\mathsf{h}}{\mathsf{p}}(g - \nabla_h u_{hp}\cdot \boldsymbol{n} + iku_{hp})\|_{0,\partial\Omega}.\end{aligned} \tag{3.5}$$

Proof. We follow the general ideas of the proof of [12, Theorem 3.3]. However, in order to connect with the shifted Poisson problem (3.1), some extra terms need to be bounded. We repeat the full proof for completeness.

Let $s \in H^1_*(\Omega)$ be defined by the projection

$$(\nabla s, \nabla v) = (\mathcal{G}(u_{hp}), \nabla v) \quad \text{for all } v \in H^1(\Omega). \tag{3.6}$$

Then, by orthogonality, we have that

$$\|\nabla u - \mathcal{G}(u_{hp})\|^2_{0,\Omega} = \|\nabla(u - s)\|^2_{0,\Omega} + \|\nabla s - \mathcal{G}(u_{hp})\|^2_{0,\Omega}. \tag{3.7}$$

Since $s \in H^1_*(\Omega)$ is the orthogonal projection, we have that

$$\|\nabla s - \mathcal{G}(u_{hp})\|_{0,\Omega} = \min_{v\in H^1_*(\Omega)} \|\nabla v - \mathcal{G}(u_{hp})\|_{0,\Omega}.$$

Hence, for any $s_{hp} \in H^1_*(\Omega)$, we get the following bound for the second term in (3.7):

$$\|\nabla s - \mathcal{G}(u_{hp})\|^2_{0,\Omega} \le \|\nabla s_{hp} - \mathcal{G}(u_{hp})\|^2_{0,\Omega}. \tag{3.8}$$

The first term of (3.7) is estimated by the flux reconstruction as follows. We have

$$\begin{aligned}\|\nabla(u - s)\|_{0,\Omega} &= \sup_{v\in H^1_*(\Omega),\, \|\nabla v\|_{0,\Omega}=1} (\nabla(u - s), \nabla v) \\ &= \sup_{v\in H^1_*(\Omega),\, \|\nabla v\|_{0,\Omega}=1} (\nabla u - \mathcal{G}(u_{hp}), \nabla v),\end{aligned}$$

where the second identity follows from (3.6). Adding and subtracting an equilibrated flux reconstruction $\boldsymbol{\sigma}_{hp} \in H(\mathrm{div};\Omega)$ leads to

$$(\nabla u - \mathcal{G}(u_{hp}), \nabla v) = (\nabla u + \boldsymbol{\sigma}_{hp}, \nabla v) - (\mathcal{G}(u_{hp}) + \boldsymbol{\sigma}_{hp}, \nabla v). \tag{3.9}$$

Using the weak formulation (2.1) and integrating by parts in the first term on the right-hand side of (3.9) yields, for any $v \in H^1_*(\Omega)$ with $\|\nabla v\|_{0,\Omega} = 1$,

$$\begin{aligned}(\nabla u + \boldsymbol{\sigma}_{hp}, \nabla v) &= (\nabla u, \nabla v) + (\boldsymbol{\sigma}_{hp}, \nabla v) \\ &= (f + k^2 u - \mathrm{div}\,\boldsymbol{\sigma}_{hp}, v) + (g + iku + \boldsymbol{\sigma}_{hp}\cdot\boldsymbol{n}, v)_{\partial\Omega} \\ &= (f + k^2 u_{hp} - \mathrm{div}\,\boldsymbol{\sigma}_{hp}, v) + (g + iku_{hp} + \boldsymbol{\sigma}_{hp}\cdot\boldsymbol{n}, v)_{\partial\Omega} \\ &\quad + k^2(u - u_{hp}, v) + ik(u - u_{hp}, v)_{\partial\Omega}.\end{aligned} \tag{3.10}$$

Here, the proof differs from that of [12, Theorem 3.3], in that we introduce the last two extra terms. From Definition 3.1 of the equilibrated flux reconstruction $\boldsymbol{\sigma}_{hp}$, we get for the first term on the right-hand side of (3.10), for each element $T \in \mathcal{T}$, that

$$
\begin{aligned}
(f + k^2 u_{hp} - \operatorname{div} \boldsymbol{\sigma}_{hp}, v)_T &= (f + k^2 u_{hp} - \operatorname{div} \boldsymbol{\sigma}_{hp}, v - \Pi_T^0 v)_T \\
&\leq \|f + k^2 u_{hp} - \operatorname{div} \boldsymbol{\sigma}_{hp}\|_{0,T} \|v - \Pi_T^0 v\|_{0,T} \\
&\leq \frac{h_T}{j_{1,1}} \|f + k^2 u_{hp} - \operatorname{div} \boldsymbol{\sigma}_{hp}\|_{0,T} \|\nabla v\|_{0,T},
\end{aligned}
$$

where in the last step we have used the bound (3.3). For the second term on the right-hand side of (3.10), we write

$$
\begin{aligned}
&(g + iku_{hp} + \boldsymbol{\sigma}_{hp} \cdot \boldsymbol{n}, v)_{\partial\Omega} \\
&\quad = (\boldsymbol{\sigma}_{hp} \cdot \boldsymbol{n} + g + iku_{hp} - \gamma k \frac{\mathsf{h}}{\mathsf{p}} (g - \nabla_h u_{hp} \cdot \boldsymbol{n} - iku_{hp}), v)_{\partial\Omega} \\
&\qquad + (\gamma k \frac{\mathsf{h}}{\mathsf{p}} (g - \nabla_h u_{hp} \cdot \boldsymbol{n} - iku_{hp}), v)_{\partial\Omega},
\end{aligned}
$$

where we need to introduce the last term in order to connect to the shifted Poisson problem (3.1). Again, from the definition of $\boldsymbol{\sigma}_{hp}$, for any boundary edge E belonging to the triangle T, we have that

$$
\begin{aligned}
&\left(\boldsymbol{\sigma}_{hp} \cdot \boldsymbol{n} + g + iku_{hp} - \gamma k \frac{\mathsf{h}}{\mathsf{p}} (g - \nabla_h u_{hp} \cdot \boldsymbol{n} - iku_{hp}), v \right)_E \\
&\quad = \left(\boldsymbol{\sigma}_{hp} \cdot \boldsymbol{n} + g + iku_{hp} - \gamma k \frac{\mathsf{h}}{\mathsf{p}} (g - \nabla_h u_{hp} \cdot \boldsymbol{n} - iku_{hp}), v - \Pi_T^0 v \right)_E \\
&\quad \leq \left\| \boldsymbol{\sigma}_{hp} \cdot \boldsymbol{n} + g + iku_{hp} - \gamma k \frac{\mathsf{h}}{\mathsf{p}} (g - \nabla_h u_{hp} \cdot \boldsymbol{n} - iku_{hp}) \right\|_{0,E} \|v - \Pi_T^0 v\|_{0,E} \\
&\quad \leq C_{tr} h_E^{1/2} \left\| \boldsymbol{\sigma}_{hp} \cdot \boldsymbol{n} + g + iku_{hp} - \gamma k \frac{\mathsf{h}}{\mathsf{p}} (g - \nabla_h u_{hp} \cdot \boldsymbol{n} - iku_{hp}) \right\|_{0,E} \|\nabla v\|_{0,T},
\end{aligned}
$$

where in the last step we have used the bound from Lemma 3.4.

From the Cauchy–Schwarz inequality, the above estimates, the Poincaré and trace estimates, and

$$
(\mathcal{G}(u_{hp}) + \boldsymbol{\sigma}_{hp}, \nabla v)_T \leq \|\mathcal{G}(u_{hp}) + \boldsymbol{\sigma}_{hp}\|_{0,T} \|\nabla v\|_{0,T},
$$

noting that $\|\nabla v\|_{0,\Omega} = 1$, we deduce the bound

$$
\begin{aligned}
(\nabla u - \mathcal{G}(u_{hp}), \nabla v) \lesssim \eta_{hp} &+ k^2 \|u - u_{hp}\|_{0,\Omega} + k \|u - u_{hp}\|_{0,\partial\Omega} \\
&+ \|\gamma k \frac{\mathsf{h}}{\mathsf{p}} (g - \nabla_h u_{hp} \cdot \boldsymbol{n} - iku_{hp})\|_{0,\partial\Omega}
\end{aligned}
$$

for (3.9). Then, inserting this bound and (3.8) into (3.7) completes the proof. ∎

Remark 3.7. Assuming that the resolution conditions established in [23] are satisfied, and that an appropriate mesh refinement near the domain corners is applied, the L^2 error terms appearing on the right-hand side of the reliability bound (3.5) in Theorem 3.6 are actually higher-order terms, compared to the left-hand side.

4. Efficiency of the error estimator. The result in the previous section holds for any equilibrated flux and potential reconstructions; cf. Definitions 3.1 and 3.2, respectively. In this section, we *locally* define equilibrated flux and potential reconstructions, for which we can show that the error estimator (3.4) is efficient.

In section 4.1, we start by constructing equilibrated fluxes on nodal patches by solving local mixed problems with Raviart–Thomas finite elements. We then show that the sum of these local fluxes satisfies the definition of an admissible flux reconstruction (see Definition 3.1). We prove the efficiency of this flux reconstruction in Theorem 4.6 below. The technique of this proof involves two steps: an estimate for the strong residual, and the p-robustness of the mixed approximation (see Lemmas 4.4 and 4.5, respectively).

In section 4.2, we construct local potentials by solving minimization problems again on nodal patches. We reformulate these minimization problems as coercive variational problems, which can only be done in two dimensions. By combining these local potentials, we construct an admissible potential reconstruction, according to Definition 3.2, and prove its efficiency (see Theorem 4.7).

In section 4.3, we show the efficiency of the remaining data terms and state the final efficiency result.

4.1. Localized equilibrated flux reconstruction. We first define a computable equilibrated flux reconstruction $\boldsymbol{\sigma}_{hp}$, such that the terms in the error estimator (3.4) containing this reconstruction are efficient.

Using the partition of unity property of the linear hat functions, we can localize the construction of $\boldsymbol{\sigma}_{hp}$ on nodal patches ω_z by solving local patch problems in mixed formulations. For a given node $z \in \mathcal{N}$, with given integer $p_z \geq 1$, we define the space

$$\Sigma_{hp}(\omega_z) := \{\boldsymbol{\tau}_{hp} \in H(\mathrm{div}, \omega_z) \,:\, \boldsymbol{\tau}_{hp}|_T \in RT_{p_z}(T) \text{ for all } T \in \mathcal{T}(z)\}$$

of Raviart–Thomas finite elements $RT_{p_z}(T) := \left\{[\mathbb{P}_{p_z}(T)]^2 + \widetilde{\mathbb{P}}_{p_z}(T)[x_1, x_2]^t\right\}$, where $\widetilde{\mathbb{P}}_{p_z}(T)$ is the space of homogeneous polynomials of degree p_z, and the space

$$Q_{hp}(\omega_z) = \{q_{hp} \in L^2(\omega_z) : q_{hp}|_T \in \mathbb{P}_{p_z}(T) \text{ for all } T \in \mathcal{T}(z)\}.$$

Let $\psi_z \in H^1(\Omega)$ denote the piecewise linear hat function for the vertex $z \in \mathcal{N}$ with patch ω_z. Inserting ψ_z as test functions into the discrete weak formulation (2.3), we get, via straightforward calculations, the following hat function orthogonality:

$$\begin{aligned}
&(\mathcal{G}(u_{hp}), \nabla\psi_z)_{\omega_z} - (f + k^2 u_{hp}, \psi_z)_{\omega_z} \\
&\qquad = (g + iku_{hp}, \psi_z)_{\partial\omega_z \cap \partial\Omega} - \left(\gamma k \frac{\mathsf{h}}{\mathsf{p}}(g - \nabla_h u_{hp} \cdot \boldsymbol{n} + iku_{hp}), \psi_z\right)_{\partial\omega_z \cap \partial\Omega} \\
&\qquad\quad - i\gamma \frac{\mathsf{h}}{\mathsf{p}} \left(g - \nabla_h u_{hp} \cdot \boldsymbol{n} + iku_{hp}, \nabla_h \psi_z \cdot \boldsymbol{n}\right)_{\partial\omega_z \cap \partial\Omega}.
\end{aligned} \tag{4.1}$$

Define, for $z \in \mathcal{N}$ and a given function $g^z \in L^2(\partial\omega_z \cap \partial\Omega)$, the local mixed finite element spaces

$$\begin{aligned}
\Sigma^z_{g^z,hp} &:= \{\boldsymbol{\tau}_{hp} \in \Sigma_{hp}(\omega_z) \,:\, \boldsymbol{\tau}_{hp} \cdot \boldsymbol{n} = 0 \text{ on } \partial\omega_z \backslash \partial\Omega, \\
&\qquad\qquad \boldsymbol{\tau}_{hp} \cdot \boldsymbol{n}|_E = \Pi^{p_z}_E g^z \text{ for all } E \subset \partial\omega_z \cap \partial\Omega\}, \\
Q^z_{hp} &:= \{q_{hp} \in Q_{hp}(\omega_z) \,:\, (q_{hp}, 1)_{\omega_z} = 0\}.
\end{aligned}$$

For each node $z \in \mathcal{N}$, we solve the following local problem in mixed form: Find an approximation $(\boldsymbol{\zeta}^z_{hp}, r^z_{hp}) \in \Sigma^z_{g^z,hp} \times Q^z_{hp}$ such that

$$\begin{aligned}
(\boldsymbol{\zeta}^z_{hp}, \boldsymbol{\tau}_{hp})_{\omega_z} - (r^z_{hp}, \mathrm{div}\, \boldsymbol{\tau}_{hp})_{\omega_z} &= -(\psi_z \mathcal{G}(u_{hp}), \boldsymbol{\tau}_{hp})_{\omega_z} \quad \text{for all } \boldsymbol{\tau}_{hp} \in \Sigma^z_{0,hp}, \\
(\mathrm{div}\, \boldsymbol{\zeta}^z_{hp}, q_{hp})_{\omega_z} &= (f^z, q_{hp})_{\omega_z} \qquad\qquad \text{for all } q_{hp} \in Q^z_{hp},
\end{aligned} \tag{4.2}$$

where the function f^z is given by

$$f^z := (f + k^2 u_{hp})\psi_z - \mathcal{G}(u_{hp}) \cdot \nabla \psi_z, \tag{4.3}$$

and the function $g^z \in L^2(\partial\omega_z \cap \partial\Omega)$ in the definition of $\Sigma^z_{g^z,h}$ is given by

$$\begin{aligned} g^z := &- \left(g + iku_{hp} - \gamma k \frac{\mathsf{h}}{\mathsf{p}} (g - \nabla_h u_{hp} \cdot \boldsymbol{n} + iku_{hp}) \right) \psi_z \\ &+ i\gamma \frac{\mathsf{h}}{\mathsf{p}} \left(g - \nabla_h u_{hp} \cdot \boldsymbol{n} + iku_{hp} \right) \left(\nabla_h \psi_z \cdot \boldsymbol{n} \right). \end{aligned} \tag{4.4}$$

Actually, f^z and g^z are defined such that, from the hat function orthogonality (4.1), we get

$$(f^z, 1)_{\omega_z} = (g^z, 1)_{\partial\omega_z \cap \partial\Omega}, \tag{4.5}$$

which is the pure Neumann problem compatibility condition.

Remark 4.1. From integration by parts, the boundary condition on $\partial\omega_z$, and the compatibility condition (4.5), we note that

$$(\operatorname{div} \boldsymbol{\zeta}^z_{hp}, 1)_{\omega_z} = \int_{\partial\omega_z} \boldsymbol{\zeta}^z_{hp} \cdot \boldsymbol{n} \, dx = \int_{\partial\omega_z \cap \partial\Omega} g^z \, dx = (f^z, 1)_{\omega_z}.$$

Hence, together with (4.2), we have that

$$(\operatorname{div} \boldsymbol{\zeta}^z_{hp}, q_{hp})_{\omega_z} = (f^z, q_{hp})_{\omega_z} \qquad \text{for all } q_{hp} \in Q_{hp}(\omega_z). \tag{4.6}$$

We can now define the equilibrated flux reconstruction $\boldsymbol{\sigma}_{hp}$ as

$$\boldsymbol{\sigma}_{hp} := \sum_{z \in \mathcal{N}} \boldsymbol{\zeta}^z_{hp} \tag{4.7}$$

and prove that it satisfies Definition 3.1.

LEMMA 4.2. *The flux approximation $\boldsymbol{\sigma}_{hp}$, defined in* (4.7)*, is an equilibrated flux reconstruction in $H(\operatorname{div};\Omega)$ which satisfies, for any $T \in \mathcal{T}$,*

$$(f + k^2 u_{hp} - \operatorname{div} \boldsymbol{\sigma}_{hp}, q_{hp})_T = 0$$

for all $q_{hp} \in \bigcap_{z \in \mathcal{N}(T)} Q_{hp}(\omega_z)|_T$ and satisfies, for any $E \in \mathcal{E}(\partial\Omega)$,

$$\left(\boldsymbol{\sigma}_{hp} \cdot \boldsymbol{n} + g + iku_{hp} - \gamma k \frac{\mathsf{h}}{\mathsf{p}} (g - \nabla_h u_{hp} \cdot \boldsymbol{n} + iku_{hp}), q_{hp} \right)_E = 0$$

for all $q_{hp} \in \bigcap_{z \in \mathcal{N}(E)} Q_{hp}(\omega_z)|_E$.

Proof. For all $z \in \mathcal{N}$, by the extension of $\boldsymbol{\zeta}^z_{hp}$ by zero in $\Omega \setminus \omega_z$, we have that $\boldsymbol{\zeta}^z_{hp} \in H(\operatorname{div};\Omega)$; therefore, $\boldsymbol{\sigma}_{hp} \in H(\operatorname{div};\Omega)$ also holds. For any $T \in \mathcal{T}$, by using the partition of unity property of ψ_z, the definition of $\boldsymbol{\sigma}_{hp}$, and (4.6), it holds that

$$
\begin{aligned}
(f + k^2 u_{hp} - \operatorname{div} \boldsymbol{\sigma}_{hp}, q_{hp})_T &= \sum_{z \in \mathcal{N}(T)} (\psi_z (f + k^2 u_{hp}) - \operatorname{div} \boldsymbol{\zeta}_{hp}^z, q_{hp})_T \\
&= \sum_{z \in \mathcal{N}(T)} (\mathcal{G}(u_{hp}) \cdot \nabla \psi_z, q_{hp})_T \\
&= 0
\end{aligned}
$$

for all $q_{hp} \in Q_{hp}$, where in the last step we used the fact that $\sum_{z \in \mathcal{N}(T)} \nabla \psi_z = 0$. Using the partition of unity property of ψ_z along the boundary edges, the definition of $\boldsymbol{\sigma}_{hp}$, and the fact that $\boldsymbol{\zeta}_{hp}^z \in \Sigma_{g^z, hp}^z$, we get for any $E \in \mathcal{E}(\partial\Omega)$, with associated element $T_E \in \mathcal{T}$, that

$$
\begin{aligned}
(\boldsymbol{\sigma}_{hp} \cdot \boldsymbol{n}, q_{hp})_E &= \sum_{z \in \mathcal{N}(T_E)} (\boldsymbol{\zeta}_{hp}^z \cdot \boldsymbol{n}, q_{hp})_E = \sum_{z \in \mathcal{N}(T_E)} (g^z, q_{hp})_E \\
&= \left(-(g + iku_{hp}) + \gamma k \frac{\mathsf{h}}{\mathsf{p}} (g - \nabla_h u_{hp} \cdot \boldsymbol{n} + iku_{hp}), q_{hp} \right)_E
\end{aligned}
$$

for all $q_{hp} \in Q_{hp}$, where we use the fact that $\sum_{z \in \mathcal{N}(T_E)} \psi_z = 1$ and the fact that $\sum_{z \in \mathcal{N}(T_E)} \nabla \psi_z \cdot \boldsymbol{n} = 0$ on E. ∎

We proceed by showing that the flux reconstruction (4.7) is efficient. In order to do that, we start by defining the following data oscillation terms.

DEFINITION 4.3 (data oscillations). *We define*

$$
\begin{aligned}
\operatorname{osc}^2(f^z) &= \sum_{T \in \mathcal{T}(z)} \frac{h_T^2}{j_{1,1}^2} \| f^z - \Pi_T^{p_z} f^z \|_{0,T}^2, \\
\operatorname{osc}^2(g^z) &= \sum_{E \in \mathcal{E}(z) \cap \mathcal{E}(\partial\Omega)} C_{tr}^2 h_E \| g^z - \Pi_E^{p_z} g^z \|_{0,E}^2
\end{aligned}
$$

for all $z \in \mathcal{N}$ and

$$
\operatorname{osc}^2(f) = \sum_{z \in \mathcal{N}} \operatorname{osc}^2(f^z), \qquad \operatorname{osc}^2(g) = \sum_{z \in \mathcal{N}(\partial\Omega)} \operatorname{osc}^2(g^z).
$$

Now, we derive an estimate of the strong residual. The following lemma is based on the results in [7].

LEMMA 4.4 (continuous efficiency, flux reconstruction). *Let w be the weak solution of the (shifted) Poisson problem* (3.1)*, with $u_{hp} \in V_{hp}$ being the hp-DG approximation given by* (2.3)*. Furthermore, let $z \in \mathcal{N}$ and $r^z \in H_*^1(\omega_z) := \{v \in H^1(\omega_z) : (v, 1)_{\omega_z} = 0\}$ be the solution to the continuous problem*

$$
\begin{aligned}
(\nabla r^z, \nabla v)_{\omega_z} = &-(\psi_z \mathcal{G}(u_{hp}), \nabla v)_{\omega_z} + \sum_{T \in \mathcal{T}(z)} (\Pi_T^{p_z} f^z, v)_T \\
&- \sum_{E \in \mathcal{E}(z) \cap \mathcal{E}(\partial\Omega)} (\Pi_E^{p_z} g^z, v)_E
\end{aligned} \tag{4.8}
$$

for all $v \in H^1(\omega_z)$, with the right-hand side f^z and the boundary function g^z given in (4.3) *and* (4.4)*, respectively. Then, it holds that*

$$
\begin{aligned}
\| \nabla r^z \|_{0,\omega_z} \lesssim \| \nabla w - \mathcal{G}(u_{hp}) \|_{0,\omega_z} &+ \left\| i\gamma \frac{\sqrt{\mathsf{h}}}{\mathsf{p}} (g - \nabla_h u_{hp} \cdot \boldsymbol{n} + iku_{hp}) \right\|_{0, \partial\omega_z \cap \partial\Omega} \\
&+ \operatorname{osc}(f^z) + \operatorname{osc}(g^z).
\end{aligned}
$$

Proof. Since the right-hand side f^z and the boundary function g^z are constructed such that the compatibility condition (4.5) is satisfied on ω_z, it is therefore also satisfied for their L^2-projections. This, together with the Lax–Milgram lemma, implies that (4.8) is well posed. We have that

$$\|\nabla r^z\|_{0,\omega_z} = \sup_{v\in H^1_*(\omega_z),\|\nabla v\|_{0,\omega_z}=1} (\nabla r^z,\nabla v)_{\omega_z}; \tag{4.9}$$

moreover, for $v \in H^1_*(\omega_z)$, $\|\nabla v\|_{0,\omega_z} = 1$, we can write

$$\begin{aligned}(\nabla r^z,\nabla v)_{\omega_z} &= -(\psi_z\mathcal{G}(u_{hp}),\nabla v)_{\omega_z} + \sum_{T\in\mathcal{T}(z)} (\Pi_T^{p_z} f^z, v)_T - \sum_{E\in\mathcal{E}(z)\cap\mathcal{E}(\partial\Omega)} (\Pi_E^{p_z} g^z, v)_E\\ &= -(\psi_z\mathcal{G}(u_{hp}),\nabla v)_{\omega_z} + (f^z,v)_{\omega_z} - (g^z,v)_{\partial\omega_z\cap\partial\Omega}\\ &\quad + \sum_{T\in\mathcal{T}(z)} (\Pi_T^{p_z} f^z - f^z, v-\Pi_T^0 v)_T - \sum_{E\in\mathcal{E}(z)\cap\mathcal{E}(\partial\Omega)} (\Pi_E^{p_z} g^z - g^z, v-\Pi_T^0 v)_E.\end{aligned}$$

The last two terms on the right-hand side are bounded by $\operatorname{osc}(f^z)$ and $\operatorname{osc}(g^z)$, respectively, by applying the Cauchy–Schwarz inequality, Lemmas 3.4 and 3.3, and the fact that $\|\nabla v\|_{0,\omega_z} = 1$. For the first three terms on the right-hand side, by the application of integration by parts, the Cauchy–Schwarz inequality, and the definitions of f^z, g^z, and w, we obtain

$$\begin{aligned}&-(\psi_z\mathcal{G}(u_{hp}),\nabla v)_{\omega_z} + (f^z,v)_{\omega_z} - (g^z,v)_{\partial\omega_z\cap\partial\Omega}\\ &\quad= -(\psi_z\mathcal{G}(u_{hp}),\nabla v)_{\omega_z} + ((f+k^2u_{hp})\psi_z, v)_{\omega_z} - (\mathcal{G}(u_{hp})\cdot\nabla\psi_z, v)_{\omega_z}\\ &\qquad - (g^z,v)_{\partial\omega_z\cap\partial\Omega}\\ &\quad= (\nabla w - \mathcal{G}(u_{hp}), \nabla_h(\psi_z v))_{\omega_z}\\ &\qquad - \left(i\gamma\frac{\mathsf{h}}{\mathsf{p}}\left(g-\nabla_h u_{hp}\cdot\boldsymbol{n}+iku_{hp}\right)(\nabla_h\psi_z\cdot\boldsymbol{n}), v\right)_{\partial\omega_z\cap\partial\Omega}\\ &\quad\le \|\nabla w - \mathcal{G}(u_{hp})\|_{0,\omega_z}\|\nabla_h(\psi_z v)\|_{0,\omega_z}\\ &\qquad + \left\|i\gamma\frac{\sqrt{\mathsf{h}}}{\mathsf{p}}\left(g-\nabla_h u_{hp}\cdot\boldsymbol{n}+iku_{hp}\right)\right\|_{0,\partial\omega_z\cap\partial\Omega}\|\sqrt{\mathsf{h}}(\nabla_h\psi_z\cdot\boldsymbol{n})v\|_{0,\partial\omega_z\cap\partial\Omega}.\end{aligned}$$

By the triangle inequality, the scaling of the hat functions, shape regularity, and the Poincaré inequality, we have that

$$\|\nabla_h(\psi_z v)\|_{0,\omega_z} \le \|v\nabla_h\psi_z\|_{0,\omega_z} + \|\psi_z\nabla v\|_{0,\omega_z} \lesssim \|\mathsf{h}v\|_{0,\omega_z} + \|\nabla v\|_{0,\omega_z} \lesssim \|\nabla v\|_{0,\omega_z} = 1;$$

a similar bound holds for $\|\sqrt{\mathsf{h}}(\nabla_h\psi_z\cdot\boldsymbol{n})v\|_{0,\partial\omega_z\cap\partial\Omega}$ after the application of shape regularity and the trace estimates. Therefore, we conclude from the previous estimates that

$$\begin{aligned}(\nabla r^z,\nabla v)_{\omega_z} &\lesssim \|\nabla w - \mathcal{G}(u_{hp})\|_{0,\omega_z}\\ &\qquad + \left\|i\gamma\frac{\sqrt{\mathsf{h}}}{\mathsf{p}}\left(g-\nabla_h u_{hp}\cdot\boldsymbol{n}+iku_{hp}\right)\right\|_{0,\partial\omega_z\cap\partial\Omega} + \operatorname{osc}(f^z) + \operatorname{osc}(g^z)\end{aligned}$$

for all $v \in H^1_*(\omega_z)$ such that $\|\nabla v\|_{0,\omega_z} = 1$. Inserting this result into (4.9) completes the proof. ∎

In the following lemma, we essentially report [4, Theorem 7], which is a key result in the proof of p-robustness.

LEMMA 4.5. *Let $u_{hp} \in V_{hp}$ be the hp-DG approximation given by* (2.3)*; furthermore, for $z \in \mathcal{N}$, let $\boldsymbol{\zeta}_{hp}^z \in \Sigma_{g^z,hp}^z$ be the solution to the local nodal mixed problem* (4.2)*, $\psi_z \in H^1(\Omega)$ be the nodal hat function associated with the node z, and $r^z \in H_*^1(\omega_z)$ be defined as in Lemma* 4.4*. Then, the stability result*

$$\|\psi_z \mathcal{G}(u_{hp}) + \boldsymbol{\zeta}_{hp}^z\|_{0,\omega_z} \leq C \|\nabla r^z\|_{0,\omega_z}$$

holds, with a constant $C > 0$ that is independent of the polynomial degree, mesh size, and wave number but depends on the shape regularity of the mesh.

Proof. As in [12, Corollary 3.16], the proof is essentially [4, Theorem 7]. Note that

$$\|\nabla r^z\|_{0,\omega_z} = \sup_{v \in H_*^1(\omega_z),\, \|\nabla v\|_{0,\omega_z}=1} (\nabla r^z, \nabla v)_{\omega_z}.$$

In fact, from (4.8) we have that

$$\begin{aligned}(\nabla r^z, \nabla v)_{\omega_z} &= -(\psi_z \mathcal{G}(u_{hp}), \nabla v)_{\omega_z} + \sum_{T \in \mathcal{T}(z)} (\Pi_T^{p_z} f^z, v)_T - \sum_{E \in \mathcal{E}(z) \cap \mathcal{E}(\partial\Omega)} (\Pi_E^{p_z} g^z, v)_E \\ &= \sum_{T \in \mathcal{T}(z)} \int_T (\operatorname{div}(\psi_z \mathcal{G}(u_{hp})) + \Pi_T^{p_z} f^z) v \, dx + \sum_{E \in \mathcal{E}(z) \cap \mathcal{E}(\Omega)} \int_E [\![-\psi_z \mathcal{G}(u_{hp})]\!]_N v \, ds \\ &\quad - \sum_{E \in \mathcal{E}(z) \cap \mathcal{E}(\partial\Omega)} \int_E (\Pi_E^{p_z} g^z + \psi_z \mathcal{G}(u_{hp})) v \, ds\end{aligned}$$

for all $v \in H_*^1(\omega_z)$ such that $\|\nabla v\|_{0,\omega_z} = 1$.

Defining $r_T := \operatorname{div}(\psi_z \mathcal{G}(u_{hp})) + \sum_{T \in \mathcal{T}(z)} \Pi_T^{p^z} f^z$, $r_E := [\![-\psi_z \mathcal{G}(u_{hp})]\!]_N$ for interior edges and $r_E := -\sum_{E \in \mathcal{E}(z) \cap \mathcal{E}(\partial\Omega)} (\Pi_E^{p_z} g^z + \psi_z \mathcal{G}(u_{hp}))$ for edges on the boundary, we have that $\|\nabla r^z\|_{0,\omega_z}$ in our notation is $\|r\|_{[H^1(\omega)\setminus\mathbb{R}]}$ in the notation of [4, Lemma 7]. Moreover,

$$\|\psi_z \mathcal{G}(u_{hp}) + \boldsymbol{\zeta}_{hp}^z\|_{0,\omega_z} = \inf_{\substack{\boldsymbol{\tau}_{hp} \in \Sigma_{g^z,hp}^z \\ \operatorname{div}(\boldsymbol{\tau}_{hp})|_T = \Pi_T^{p_z} f^z \text{ for all } T \in \mathcal{T}(z)}} \|\psi_z \mathcal{G}(u_{hp}) + \boldsymbol{\tau}_{hp}\|_{0,\omega_z},$$

which, in the notation of [4], reads as

$$\inf_{\sigma \in \mathrm{RT}_{-1,0}^p,\, \operatorname{div}\sigma = r} \|\sigma\|_0,$$

formulated in the broken Raviart–Thomas finite element space with imposed jumps $[\![-\psi_z \mathcal{G}(u_{hp})]\!]_N$. ∎

Finally, by using Lemmas 4.4 and 4.5, we prove a p-robust efficiency bound of the first term in the error estimator (3.4).

THEOREM 4.6 (flux reconstruction efficiency). *Let $u \in H^1(\Omega)$ be the weak solution of the Helmholtz problem* (2.1)*, $u_{hp} \in V_{hp}$ be the discrete solution of* (2.3)*, and $\boldsymbol{\sigma}_{hp} \in H(\operatorname{div};\Omega)$ be the equilibrated flux reconstruction of u_{hp} defined in* (4.7)*; then,*

$$\begin{aligned}\|\mathcal{G}(u_{hp}) + \boldsymbol{\sigma}_{hp}\|_{0,\Omega} \lesssim \|\nabla u - \mathcal{G}(u_{hp})\|_{0,\Omega} + k^2 \|u - u_{hp}\|_{0,\Omega} + k \|u - u_{hp}\|_{0,\partial\Omega} \\ + \operatorname{osc}(f) + \operatorname{osc}(g) + \left\| \gamma k \frac{\mathsf{h}}{\mathsf{p}} (g - \nabla_h u_{hp} \cdot \boldsymbol{n} + i k u_{hp}) \right\|_{0,\partial\Omega} \\ + \left\| i\gamma \frac{\sqrt{\mathsf{h}}}{\mathsf{p}} (g - \nabla_h u_{hp} \cdot \boldsymbol{n} + i k u_{hp}) \right\|_{0,\partial\Omega}.\end{aligned}$$

Proof. The uniform stability of the local mixed problems from Lemma 4.5 and the partition of unity property prove that

$$\|\mathcal{G}(u_{hp}) + \boldsymbol{\sigma}_{hp}\|_{0,\Omega} \leq \sum_{z\in\mathcal{N}} \|\psi_z \mathcal{G}(u_{hp}) + \boldsymbol{\zeta}_{hp}^z\|_{0,\omega_z} \leq C \sum_{z\in\mathcal{N}} \|\nabla r^z\|_{0,\omega_z}.$$

Applying Lemma 4.4, noting the finite overlap of the patches ω_z, bounds this term by $\operatorname{osc}(f)$, $\operatorname{osc}(g)$, $\|\nabla w - \mathcal{G}(u_{hp})\|_{0,\Omega}$, and the boundary terms appearing in the right-hand side of the required bound; therefore, all that remains is to bound $\|\nabla w - \mathcal{G}(u_{hp})\|_{0,\Omega}$. By the triangle inequality, we have

$$\begin{aligned} \|\nabla w - \mathcal{G}(u_{hp})\|_{0,\Omega} &\leq \|\nabla u - \mathcal{G}(u_{hp})\|_{0,\Omega} + \|\nabla(w-u)\|_{0,\Omega} \\ &= \|\nabla u - \mathcal{G}(u_{hp})\|_{0,\Omega} + \sup_{v\in H^1_*(\Omega),\, \|\nabla v\|_{0,\Omega}=1} (\nabla(w-u), \nabla v). \end{aligned} \tag{4.10}$$

Applying integration by parts, the definition of w from (3.1), (1.1), and Cauchy–Schwarz, we get that

$$\begin{aligned} (\nabla(w-u), \nabla v) &= -(\Delta(w-u), v) + (\nabla(w-u)\cdot\boldsymbol{n}, v)_{\partial\Omega} \\ &= (f + k^2 u_{hp} - (f + k^2 u), v) \\ &\quad + \left(g + iku_{hp} - \gamma k \frac{\mathsf{h}}{\mathsf{p}}(g - \nabla_h u_{hp}\cdot\boldsymbol{n} + iku_{hp}) - (g+iku), v\right)_{\partial\Omega} \\ &\leq k^2 \|u - u_{hp}\|_{0,\Omega}\|v\|_{0,\Omega} + k\|u-u_{hp}\|_{0,\partial\Omega}\|v\|_{0,\partial\Omega} \\ &\quad + \left\|\gamma k \frac{\mathsf{h}}{\mathsf{p}}(g - \nabla_h u_{hp}\cdot\boldsymbol{n} + iku_{hp})\right\|_{0,\partial\Omega} \|v\|_{0,\partial\Omega} \end{aligned}$$

for all $v \in H^1_*(\Omega)$ such that $\|\nabla v\|_{0,\Omega} = 1$. From the Poincaré inequality, we get that $\|v\|_{0,\Omega} \leq C\|\nabla v\|_{0,\Omega} = C$, where the constant C depends only on the domain Ω, and similarly by applying a trace estimate $\|v\|_{0,\partial\Omega} \leq C'\|\nabla v\|_{0,\Omega} = C'$; therefore, inserting this result into (4.10) completes the proof. ∎

4.2. Localized potential reconstruction. In this section, we define the potential reconstruction such that the error estimator (3.4) is efficient.

In order to define a localized polynomial space on patches, we need to distinguish between boundary and interior nodes. For a given boundary node $z \in \mathcal{N}(\partial\Omega)$, with associated integer $p_z \geq 1$ as defined in section 4.1, we define the localized polynomial space

$$V_{hp}^z := \{v_{hp} \in C^0(\overline{\omega_z}) \,:\, v_{hp}|_T \in \mathbb{P}_{p_z+1}(T) \quad \text{for all } T \in \mathcal{T}(z), v_{hp} = 0 \text{ on } \partial\omega_z \setminus \partial\Omega\};$$

for an internal node $z \in \mathcal{N}\setminus\mathcal{N}(\partial\Omega)$, with integer p_z, we define the localized polynomial space as

$$V_{hp}^z := \{v_{hp} \in C^0(\overline{\omega_z}) \,:\, v_{hp}|_T \in \mathbb{P}_{p_z+1}(T) \quad \text{for all } T \in \mathcal{T}(z), v_{hp} = 0 \text{ on } \partial\omega_z\}.$$

We then choose $\widetilde{s}_{hp} \in H^1(\Omega)$ as

$$\widetilde{s}_{hp} := \sum_{z\in\mathcal{N}} s_{hp}^z,$$

where

$$s_{hp}^z := \operatorname*{arg\,min}_{v_{hp}\in V_{hp}^z} \|\nabla_h(\psi_z u_{hp}) - \nabla v_{hp}\|_{0,\omega_z} \tag{4.11}$$

with extension by zero in $\Omega \setminus \omega_z$, which is equivalent to finding s_{hp}^z such that

$$(\nabla s_{hp}^z, \nabla v_{hp})_{\omega_z} = (\nabla_h(\psi_z u_{hp}), \nabla v_{hp})_{\omega_z} \quad \text{for all } v_{hp} \in V_{hp}^z.$$

Then, the potential reconstruction $s_{hp} \in H^1_*(\Omega)$ is defined as

$$s_{hp} := \widetilde{s}_{hp} - \frac{1}{|\Omega|} \int_\Omega \widetilde{s}_{hp}\, dx, \tag{4.12}$$

which clearly satisfies Definition 3.2.

It has been noted in [12, Remark 3.10] that the local minimization in (4.11) in primal form is equivalent to the following minimization in mixed form:

$$\boldsymbol{\zeta}_{hp}^z := \operatorname*{arg\,min}_{\boldsymbol{\tau}_{hp} \in \Sigma^z_{0,hp},\, \operatorname{div}(\boldsymbol{\tau}_{hp})=0} \| \mathbf{rot}_h(\psi_z u_{hp}) + \boldsymbol{\tau}_{hp}\|_{\omega_z},$$

which is equivalent to solving the following (local) mixed problem: Find $(\boldsymbol{\zeta}_{hp}^z, r_{hp}^z) \in \Sigma^z_{0,hp} \times Q^z_{hp}$ such that

$$\begin{aligned} (\boldsymbol{\zeta}_{hp}^z, \boldsymbol{\tau}_{hp})_{\omega_z} - (r_{hp}^z, \operatorname{div} \boldsymbol{\tau}_{hp})_{\omega_z} &= -(\mathbf{rot}_h(\psi_z u_{hp}), \boldsymbol{\tau}_{hp})_{\omega_z} && \text{for all } \boldsymbol{\tau}_{hp} \in \Sigma^z_{0,hp}, \\ (\operatorname{div} \boldsymbol{\zeta}_{hp}^z, q_{hp})_{\omega_z} &= 0 && \text{for all } q_{hp} \in Q^z_{hp}. \end{aligned}$$

For the underlying continuous problem, we have the following primal formulation: Find $r^z \in H^1_*(\omega_z)$ such that

$$(\nabla r^z, \nabla v)_{\omega_z} = -(\mathbf{rot}_h(\psi_z u_{hp}), \nabla v)_{\omega_z} \quad \text{for all } v \in H^1(\omega_z).$$

Proceeding as in [12, section 4.3.2] leads to the analogue of Lemma 4.4:

$$\|\nabla r^z\|^2_{0,\omega_z} \lesssim \|\nabla_h(u - u_{hp})\|^2_{0,\omega_z} + \sum_{E \in \mathcal{E}(z) \cap \mathcal{E}(\Omega)} h_E^{-1} \|\Pi_E^0 [\![u - u_{hp}]\!]_N\|^2_{0,E}.$$

Following along the lines of proof of the local efficiency in [12, Theorem 3.17] yields

$$\|\nabla_h(u_{hp} - s_{hp})\|_{0,T} \lesssim \sum_{z \in \mathcal{N}(T)} \| \mathbf{rot}_h(\psi_z u_{hp}) + \boldsymbol{\zeta}_{hp}^z\|_{0,\omega_z} \lesssim \sum_{z \in \mathcal{N}(T)} \|\nabla r^z\|_{0,\omega_z}.$$

Therefore,

$$\begin{aligned} \|\nabla_h(u_{hp} - s_{hp})\|^2_{0,T} \lesssim & \sum_{z \in \mathcal{N}(T)} \|\nabla_h(u - u_{hp})\|^2_{0,\omega_z} \\ & + \sum_{z \in \mathcal{N}(T)} \sum_{E \in \mathcal{E}(z) \cap \mathcal{E}(\Omega)} h_E^{-1} \|\Pi_E^0 [\![u - u_{hp}]\!]_N\|^2_{0,E}. \end{aligned}$$

Hence, due to the stability of the lifting operators in Lemma 2.1, we can derive the following efficiency estimate for the final term in the error estimator (3.4).

THEOREM 4.7 (potential reconstruction efficiency). *Let $u \in H^1(\Omega)$ be the weak solution of the Helmholtz problem (2.1), $u_{hp} \in V_{hp}$ be the discrete solution of (2.3), and $s_{hp} \in H^1_*(\Omega)$ be the potential reconstruction defined as in (4.12); then,*

$$\begin{aligned} \|\mathcal{G}(u_{hp}) - \nabla s_{hp}\|^2_{0,\Omega} \lesssim & \|\nabla_h(u - u_{hp})\|^2_{0,\Omega} + \sum_{E \in \mathcal{E}(\Omega)} h_E^{-1} \|\Pi_E^0 [\![u_{hp}]\!]_N\|^2_{0,E} \\ & + \sum_{E \in \mathcal{E}(\Omega)} \beta^2 h_E \|\mathsf{p}^{-1} \Pi_E^0 [\![\nabla u_{hp}]\!]_N\|^2_{0,E}. \end{aligned}$$

4.3. Efficiency result. We can now combine Theorems 4.6 and 4.7 to show that the complete error indicator (3.4) is efficient.

THEOREM 4.8 (error estimator efficiency). *Let $u \in H^1(\Omega)$ be the weak solution of the Helmholtz problem (2.1), $u_{hp} \in V_{hp}$ be the discrete solution of (2.3), η_{hp} be the error estimator (3.4), $\boldsymbol{\sigma}_{hp} \in H(\mathrm{div};\Omega)$ be the equilibrated flux reconstruction of u_{hp} defined in (4.7), and $s_{hp} \in H^1_*(\Omega)$ be the potential reconstruction defined as in (4.12); then,*

$$\begin{aligned}\eta_{hp} \lesssim{}& \|\nabla_h(u-u_{hp})\|_{0,\Omega} + k^2\|u-u_{hp}\|_{0,\Omega} + k\|u-u_{hp}\|_{0,\partial\Omega} + \mathrm{osc}(f) + \mathrm{osc}(g)\\ &+ \left\|\gamma k\frac{\mathsf{h}}{\mathsf{p}}(g-\nabla_h u_{hp}\cdot\boldsymbol{n}+iku_{hp})\right\|_{0,\partial\Omega} + \left\|i\gamma\frac{\sqrt{\mathsf{h}}}{\mathsf{p}}(g-\nabla_h u_{hp}\cdot\boldsymbol{n}+iku_{hp})\right\|_{0,\partial\Omega}\\ &+ \left(\sum_{E\in\mathcal{E}(\Omega)} h_E^{-1}\|\Pi_E^0[\![u_{hp}]\!]_N\|_{0,E}^2\right)^{1/2} + \left(\sum_{E\in\mathcal{E}(\Omega)} \beta^2 h_E\|\mathsf{p}^{-1}\Pi_E^0[\![\nabla u_{hp}]\!]_N\|_{0,E}^2\right)^{1/2}.\end{aligned}$$

Proof. The efficiency of the first and last terms of the error estimator (3.4) are given by Theorems 4.6 and 4.7, respectively, noting that

$$\begin{aligned}\|\nabla u - \mathcal{G}(u_{hp})\|_{0,\Omega} \le{}& \|\nabla_h(u-u_{hp})\|_{0,\Omega} + \left(\sum_{E\in\mathcal{E}(\Omega)} h_E^{-1}\|\Pi_E^0[\![u_{hp}]\!]_N\|_{0,E}^2\right)^{1/2}\\ &+ \left(\sum_{E\in\mathcal{E}(\Omega)} \beta^2 h_E\|\mathsf{p}^{-1}\Pi_E^0[\![\nabla u_{hp}]\!]_N\|_{0,E}^2\right)^{1/2}\end{aligned}$$

due to the triangle inequality and Lemma 2.1. Therefore, to complete the proof, we need to derive efficiency estimates for the two remaining terms of the error estimator (3.4) that contain f and g. From the partition of unity property of the hat functions ψ_z, the definition (4.3), and the property (4.6), we deduce

$$\|f + k^2u_{hp} - \mathrm{div}\,\boldsymbol{\sigma}_{hp}\|_{0,T} = \left\|\sum_{z\in\mathcal{N}(T)}(f^z - \mathrm{div}\,\boldsymbol{\xi}_{hp}^z)\right\|_{0,T} \le \sum_{z\in\mathcal{N}(T)}\|f^z - \Pi_T^{p_z}f^z\|_{0,T}.$$

Hence, summing over all $T\in\mathcal{T}$ and rearranging the summations, we arrive at

$$\sum_{T\in\mathcal{T}}\frac{h_T^2}{j_{1,1}^2}\|f + k^2u_{hp} - \mathrm{div}\,\boldsymbol{\sigma}_{hp}\|_{0,T}^2 \le \mathrm{osc}^2(f).$$

Similarly, for any boundary edge $E\in\mathcal{E}(\partial\Omega)$ with associated element $T_E\in\mathcal{T}$, we get that

$$\begin{aligned}&\left\|\boldsymbol{\sigma}_{hp}\cdot\boldsymbol{n} + g + iku_{hp} - \gamma k\frac{\mathsf{h}}{\mathsf{p}}(g-\nabla_h u_{hp}\cdot\boldsymbol{n}+iku_{hp})\right\|_{0,E}\\ &\quad= \left\|\sum_{z\in\mathcal{N}(T_E)}(\boldsymbol{\xi}_{hp}^z\cdot\boldsymbol{n} - g^z)\right\|_{0,E} \le \sum_{z\in\mathcal{N}(T_E)}\|g^z - \Pi_E^{p_z}g^z\|_{0,E},\end{aligned}$$

which proves

$$\sum_{E\in\mathcal{E}(\partial\Omega)} C_{tr}^2 h_E\left\|\boldsymbol{\sigma}_{hp}\cdot\boldsymbol{n} + g + iku_{hp} - \gamma k\frac{\mathsf{h}}{\mathsf{p}}(g-\nabla_h u_{hp}\cdot\boldsymbol{n}+iku_{hp})\right\|_{0,E}^2 \le \mathrm{osc}^2(g).$$

Combining these results completes the proof. ∎

Remark 4.9. In the numerical experiments, we will be interested in the efficiency index $\eta_{hp}/\|\nabla u - \mathcal{G}(u_{hp})\|_{0,\Omega}$ to be close to one. While we have proven the asymptotic reliability of η_{hp} for any $p_z \geq 1$, the efficiency of the flux reconstruction in Theorem 4.6 also depends on the efficiency of the data terms. Hence, for $\operatorname{osc}(f)$ and $\operatorname{osc}(g)$ to be comparably small, one has to at least match the polynomial degree p_z of the Raviart–Thomas finite element space to that of $u_{hp}\psi_z$, i.e., $p_z = \max_{T\in\mathcal{T}(z)} p_T + 1$, for the flux reconstruction. On the contrary, the efficiency of the potential reconstruction in Theorem 4.7 does not depend on the data oscillations; therefore, the choice $p_z = \max_{T\in\mathcal{T}(z)} p_T$ is sufficient in order to match the (local) polynomial degree of $u_{hp}\psi_z$ in the local minimization problems (4.11).

5. Numerical results. In this section, we present numerical results for four different benchmark problems.

For the efficiency of the error estimator, we approximate the local mixed problems with Raviart–Thomas finite elements of (varying) order $p_z = \max_{T\in\mathcal{T}(z)} p_T + 1$ for the flux reconstruction and $p_z = \max_{T\in\mathcal{T}(z)} p_T$ for the potential reconstruction; cf. Remark 4.9. To reduce the ill-conditioning of the basis for the local problems with high p_z, we use the hierarchical basis functions for the Raviart–Thomas finite element space presented in [2]. In comparison to a standard residual a posteriori error estimator, the computation of the flux and potential reconstructions is more costly; however, since all local problems are independent, they can be solved in parallel. In addition, the number of local problems is independent of the polynomial degree.

We compare p- and adaptive h-refinement to an adaptive hp-refinement strategy. For hp-refinement, we use the decision mechanism of Melenk and Wohlmuth [20, Algorithm 4.4] outlined in Algorithm 1, which determines h- or p-refinement on the refinement level ℓ based on verifying the decay of the local error indicators. We choose the constants $\gamma_h = 4$, $\gamma_p = 0.4$, $\gamma_n = 1$ and the initial values $\eta_{T,0}^{pred} = \infty$ for all $T \in \mathcal{T}$. Hence, the algorithm prefers p- over h-refinement in the first step. For mesh refinement, we use the newest vertex bisection algorithm and mark elements based on the maximum marking strategy with parameter 0.75.

Algorithm 1 *hp*-refinement algorithm.

if T is marked for refinement **then**
  if $\eta_{T,\ell} > \eta_{T,\ell}^{\mathrm{pred}}$ **then**
    Perform h-refinement: Subdivide T into 2 children $T_\pm$, and set
    $(\eta_{T_\pm,\ell+1}^{\mathrm{pred}})^2 \leftarrow \frac{1}{2}\gamma_h \left(\frac{1}{2}\right)^{p_T} \eta_{T,\ell}^2$.
  else
    Perform p-refinement: $p_T \leftarrow p_T + 1$
    $(\eta_{T,\ell+1}^{\mathrm{pred}})^2 \leftarrow \gamma_p \eta_{T,\ell}^2$
  end if
else
  $(\eta_{T,\ell+1}^{\mathrm{pred}})^2 \leftarrow \gamma_n (\eta_{T,\ell}^{\mathrm{pred}})^2$
end if

In order to shorten the pre-asymptotic region, we choose the initial mesh size h and (uniform) polynomial degree p as

$$p = \lceil \ln(k) \rceil \qquad \text{and} \qquad \frac{kh}{p} \leq C_{\mathrm{res}}, \tag{5.1}$$

where the resolution constant C_{res} depends on the problem under consideration; cf.

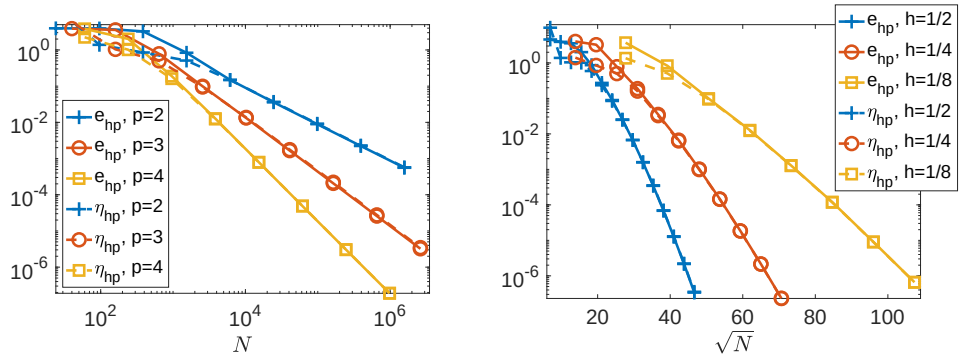

FIG. 1. *Algebraic convergence $\mathcal{O}(h^p)$ for the h-version (left) and exponential convergence of the p-version (right) of the error $e_{hp} = \|\nabla u - \mathcal{G}(u_{hp})\|_{0,\Omega}$ and the estimator η_{hp} for the example in section* 5.1 *with $k = 20$.*

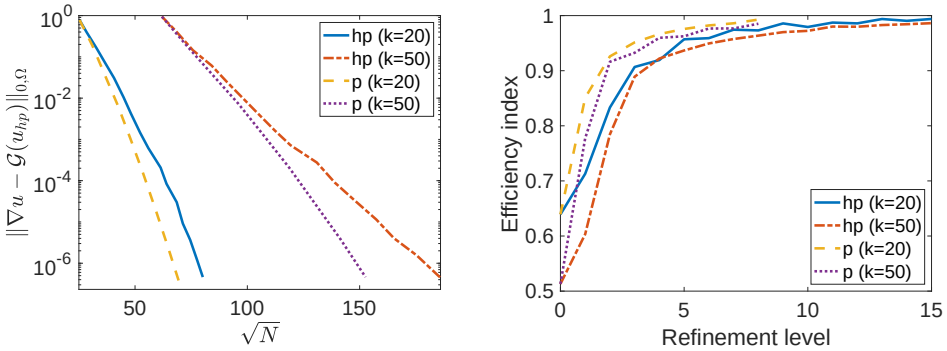

FIG. 2. *Exponential convergence (left) and efficiency indices (right) of the p- and hp-versions for the example in section* 5.1.

[23, section 5]. Additional numerical experiments, in which the initial conditions (5.1) are violated, are also presented in the following in order to demonstrate that the method under consideration is able to escape the pre-asymptotic region regardless of the initial mesh.

For the DG formulation, we choose the parameters $\alpha = 10$, $\beta = 1$, and $\gamma = 1/4$.

5.1. Square domain. Let $\Omega = (0,1)^2$, $f = 0$, and select g such that the solution of (2.1) is given by

$$u(x) = \mathcal{H}_0^{(1)}\left(k\sqrt{(x_1 + 1/4)^2 + x_2^2}\right),$$

where $\mathcal{H}_0^{(1)}$ denotes the zeroth-order Hankel function of the first kind. In Figure 1, we observe convergence of $\mathcal{O}(h^p)$, $p = 2, 3, 4$, for uniform h-refinement and exponential convergence for uniform p-refinement. Note that the error estimator is very close to the error and the corresponding lines are in fact overlapping. In Figure 2, we observe exponential convergence of the error $\|\nabla u - \mathcal{G}(u_{hp})\|_{0,\Omega}$ for both p- and adaptive hp-refinement for wave numbers $k = 20, 50$. For hp- and p-refinement, we observe efficiency indices $\eta_{hp}/\|\nabla u - \mathcal{G}(u_{hp})\|_{0,\Omega}$ asymptotically close to 1. For the construction of the initial mesh, we choose $C_{\text{res}} = 2$. Note that, for coarse h and p, the pollution

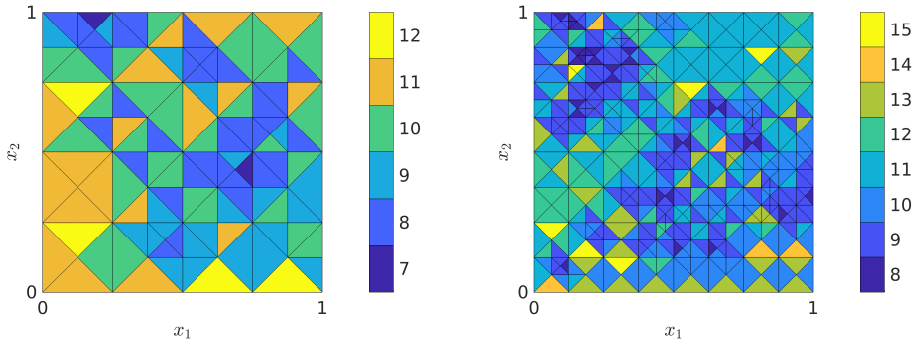

FIG. 3. *hp-refined meshes for the example in section* 5.1 *with* $k = 20$ *(left) and* $k = 50$ *(right), where the polynomial degree is indicated with different shading.*

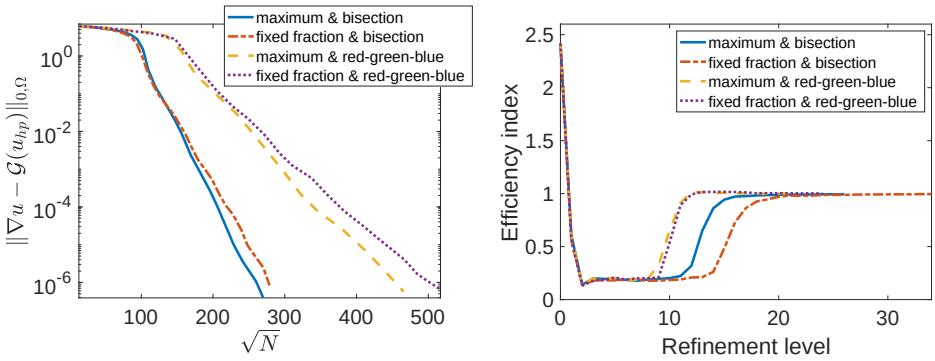

FIG. 4. *Exponential convergence (left) and efficiency indices (right) for different hp-refinement strategies for the example in section* 5.1 *with* $k = 50$.

error is still dominant and, hence, η_{hp} underestimates the error $\|\nabla u - \mathcal{G}(u_{hp})\|_{0,\Omega}$; therefore, the efficiency indices are initially less than one. The final *hp*-refined meshes for $k = 20, 50$ are displayed in Figure 3.

Next, we compare four variants of the *hp*-refinement strategy for $k = 50$. First, instead of bisecting a triangle into just two new triangles, we divide it into four using the red-green-blue-refinement strategy [24, section 4.1]. The effect of this is a more aggressive *h*-refinement. Note that our implementation of mesh refinement is based on conforming refinements, which means that there also occurs additional refinement to remove hanging nodes. This overhead is significantly larger for red-green-blue-refinement than for refinement based on bisection. The second variation is to use a fixed fraction marking strategy instead of the maximum marking strategy, where 25% of the elements with the largest indicators are refined. This leads to a more aggressive refinement between two consecutive levels. In Figure 4, we observe that less *h*-refinement is more effective; hence, the errors corresponding to refinement by bisection lead to fewer degrees of freedom than those corresponding to red-green-blue-refinement for the same level of accuracy. The two different marking strategies lead to comparable errors in this smooth example. We draw the conclusion that even though in principle we are using the same *hp*-marking strategy, the actual performance of the method depends significantly on the concrete implementation. Note that, for this

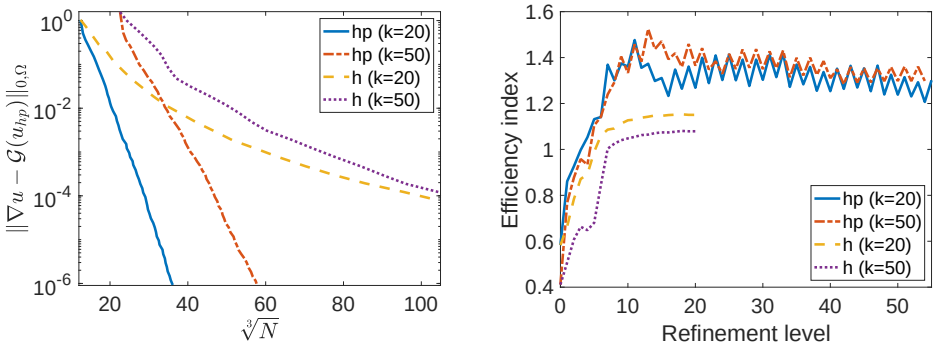

FIG. 5. *Exponential convergence (left) and efficiency indices (right) of the h- and hp-versions for the example in section* 5.2.

experiment, the choice of the initial values $p = 1$ and $h = 1/4$ violates both conditions in (5.1), and, neglecting the first mesh, the error is initially underestimated. Nevertheless, all strategies are capable of eventually refining enough so that the pollution error becomes sufficiently small, such that the efficiency indices are asymptotically close to 1 for all four strategies.

5.2. L-shaped domain. Let $\Omega = (-1,1)^2 \backslash ((0,1) \times (-1,0))$, $f = 0$, and select g such that the solution of (2.1) is given in polar coordinates (r, φ) by

$$u(r,\varphi) = \mathcal{J}_{2/3}(kr)\sin(2\varphi/3),$$

where $\mathcal{J}_{2/3}$ denotes the Bessel function of the first kind. Note that the gradient of u is singular at the origin; therefore, adaptive mesh refinement towards the origin is needed. Notice that we approximate (1.1) with $g = \nabla u \cdot \boldsymbol{n} - iku$, and g is singular at $(0,0)$. As g enters (4.2) as an essential boundary condition, we use a high polynomial degree for the flux reconstruction in the patch associated with $(0,0)$.

For the initial mesh refinement, we choose $C_{\text{res}} = 2$. In Figure 5, we observe algebraic convergence of adaptive h-refinement and exponential convergence of adaptive hp-refinement for $k = 20, 50$. More precisely, the convergence for hp-refinement is of the form $\exp(-b\sqrt[3]{N})$, and we observe that $b \approx 0.61$ for $k = 20$ and $b \approx 0.41$ for $k = 50$. This indicates that the rate of exponential convergence deteriorates for larger k. We note that higher wave numbers result in more h-refinement (cf. Figure 6) and smaller elements generally result in a slower rate of exponential convergence; cf. Figure 1. Therefore, we cannot conclude whether the rate deterioration is a direct result of the increased wave number, or is due to the increased h-refinement, which results from the higher wave number. In all cases, the efficiency indices are asymptotically close to 1.

Figure 6 displays the final hp-refined meshes for $k = 20, 50$. Note that the displayed zoom at the re-entrant corner shows low polynomial degrees close to the origin.

For comparison, in Figure 7 we compare the four variants of hp-refinement described in the previous example. We observe again that the fewer h-refinements performed by bisection is advantageous over the larger h-refinements performed by red-green-blue-refinement. For higher accuracy, the maximum marking strategy appears to be more effective than the fixed fraction marking strategy. In all four cases, the efficiency indices are asymptotically close to 1 and the four hp-strategies are

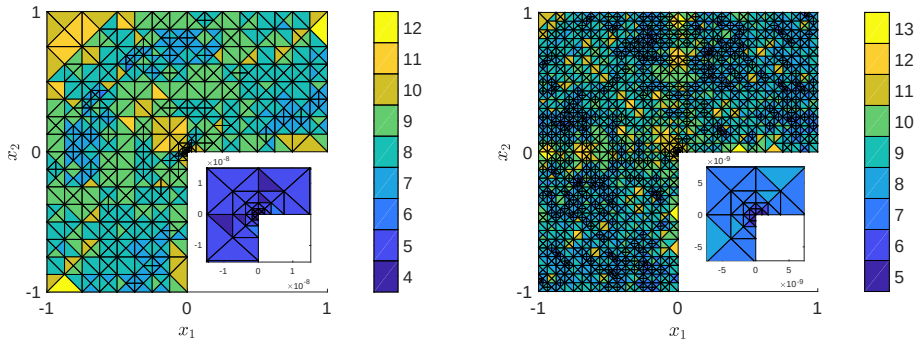

FIG. 6. *hp-refined meshes for the example in section* 5.2 *with* $k = 20$ *(left) and* $k = 50$ *(right), where the polynomial degree is indicated with different shading.*

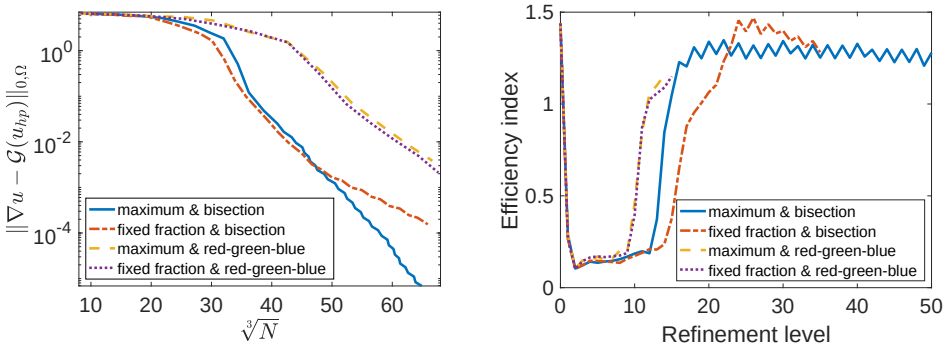

FIG. 7. *Exponential convergence (left) and efficiency indices (right) of different hp-refinement strategies for the example in section* 5.2 *with* $k = 50$.

all able to overcome the pre-asymptotic region even when starting from $p = 1$ and $h = 1/4$.

In Figure 8, we compare the equilibrated a posteriori error estimator to the residual a posteriori error estimator [23]

$$\eta^2_{hp,residual} = \sum_{T\in\mathcal{T}} \frac{h_T^2}{p_T^2}\|\Delta u_{hp} + k^2 u_{hp} + f\|^2_{0,T} + \sum_{E\in\mathcal{E}(\Omega)} \beta\frac{\mathsf{h}}{\mathsf{p}}\|[\![\nabla_h u_{hp}]\!]_N\|^2_{0,E}$$
$$+ \sum_{E\in\mathcal{E}(\Omega)} \alpha\frac{\mathsf{p}^2}{\mathsf{h}}\|[\![u_{hp}]\!]_N\|^2_{0,E} + \sum_{E\in\mathcal{E}(\partial\Omega)} \mathsf{h}\|g - \nabla_h u_{hp}\cdot\boldsymbol{n} + iku_{hp}\|^2_{0,E}.$$

We observe that the error $\|\nabla_h(u - u_{hp})\|_{0,\Omega}$ for the residual a posteriori error estimator is very close to the error $\|\nabla u - \mathcal{G}(u_{hp})\|_{0,\Omega}$ for the equilibrated a posteriori error estimator. In fact, in the case of $k = 50$, both errors overlap. The difference, however, is in the efficiency. The efficiency indices for the equilibrated a posteriori error estimator are asymptotically close to 1 and robust in p; by contrast, the efficiency indices for the residual a posteriori error estimator are close to 5 and show a small but persistent growth in p.

5.3. Internal reflection/refraction. Although not covered in the theoretical part, we now consider the benchmark from [16, section 6.3] with nonconstant refractive

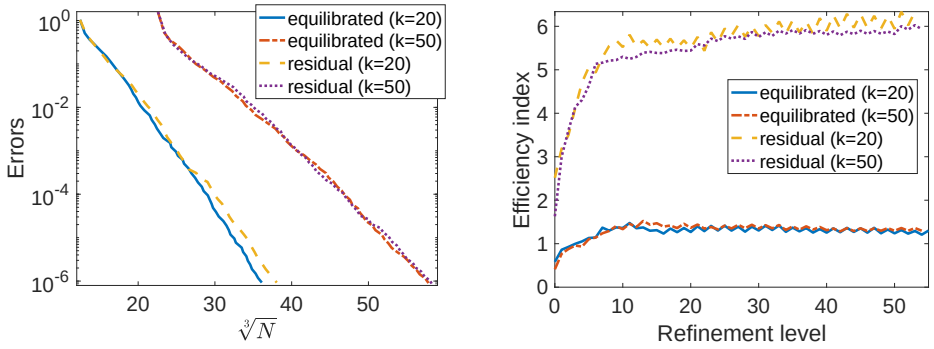

FIG. 8. *Exponential convergence (left) and efficiency indices (right) of the hp-version for the equilibrated a posteriori error estimator in comparison to the residual a posteriori error estimator for the example in section* 5.2.

index ϵ_r; hence, we consider the following problem:

$$\begin{aligned} -\Delta u - k^2 \epsilon_r u &= 0 \quad \text{in } \Omega, \\ \nabla u \cdot \boldsymbol{n} - ik\sqrt{\epsilon_r} u &= g \quad \text{on } \partial\Omega, \end{aligned}$$

where

$$\epsilon_r(x) = \begin{cases} n_1^2 & \text{if } x_2 < 0, \\ n_2^2 & \text{if } x_2 \geq 0. \end{cases}$$

For $\Omega = (-1,1)^2$, $n_1 = 2$, $n_2 = 1$, and $0 \leq \theta < \pi/2$, one can show that this problem admits the following solution:

$$u(x) = \begin{cases} (1+R)\exp\left(i(K_1 x_1 + K_3 x_2)\right) & \text{if } x_2 \geq 0, \\ \exp\left(i(K_1 x_1 + K_2 x_2)\right) + R\exp\left(i(K_1 x_1 - K_2 x_2)\right) & \text{if } x_2 < 0, \end{cases}$$

where $K_1 = kn_1\cos(\theta)$, $K_2 = kn_1\sin(\theta)$, $K_3 = k\sqrt{n_2^2 - n_1^2\cos^2(\theta)}$, and

$$R = -(K_3 - K_2)/(K_3 + K_2).$$

There exists a critical angle θ^* such that for $\theta > \theta^*$ the wave is refracted and for $\theta < \theta^*$ the wave is internally reflected; therefore, we compute two examples with $\theta_1 = 29°, 69°$, in order to demonstrate internal reflection and refraction, respectively.

The solutions for $k = 20$ and θ_1, θ_2 are displayed in Figure 9. Figures 10 and 11 show exponential convergence for both p- and adaptive hp-refinement, and the efficiency indices are again asymptotically close to 1. Note that the initial mesh is chosen such that (5.1) is fulfilled with $C_{\text{res}} = 1/2$ and the jump of the refractive index is resolved by the mesh; otherwise, strong anisotropic mesh refinement towards the interface would be needed for fast convergence. Interestingly, we observe in Figure 10 that initially hp-refinement outperforms p-refinement; however, we generally expect p-refinement to perform better, and indeed this occurs towards the end of the refinement. Figures 12 and 13 display the final hp-refined meshes for $k = 20, 50$ and θ_1 and θ_2, respectively.

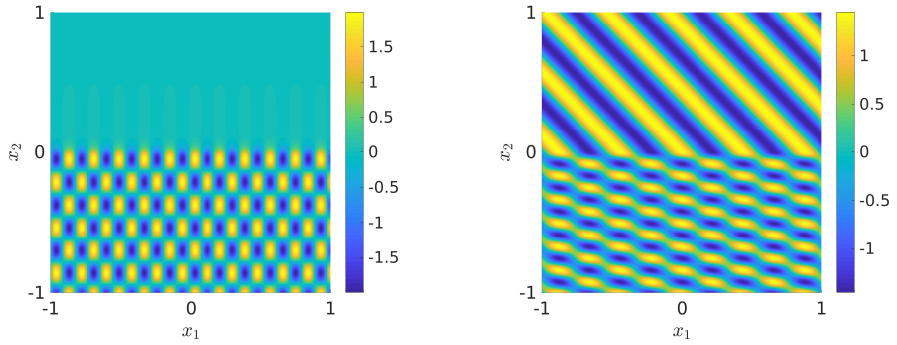

FIG. 9. *Real parts of solutions with* 29° *reflection (left) and* 69° *refraction (right) for* $k = 20$.

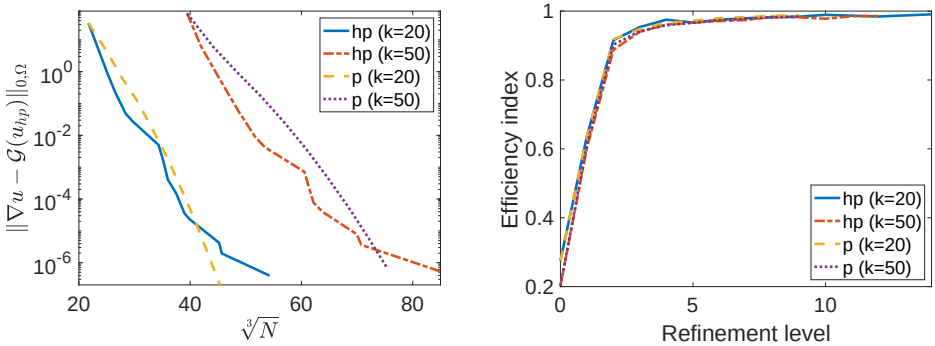

FIG. 10. *Exponential convergence (left) and efficiency indices (right) of the p- and hp-versions for the example in section* 5.3 *with* 29° *reflection.*

5.4. Gaussian beam simulation. In the last example, we consider a Gaussian beam simulation similar to the one in [22, section 3.7]. We choose the domain $\Omega = (0, 4)^2$, $f = 0$, and the inhomogeneous impedance boundary condition g corresponding to the fundamental Gaussian beam mode that satisfies the paraxial wave equation, which reads in polar coordinates as

$$v(r, \varphi) = \frac{w_0}{w} \exp\left(\frac{-r^2}{w^2} - ikz - \frac{i\pi r^2}{\lambda R} + i\theta_0\right),$$

where $z(r, \varphi)$ is the radius of the orthogonal projection of (r, φ) onto the direction of propagation, w_0 is the beam waist radius, $R(z)$ is the radius of curvature, $w(z)$ is the beam radius, and $\phi_0(z)$ is the Gaussian beam phase shift. We choose a 40° angle for the direction of the beam, and the beam waist radius $w_0 = 8\pi/k$. For the other variables, we have that $\lambda = 2\pi/k$,

$$R(z) = z + \frac{1}{z}\left(\frac{\pi w_0^2}{\lambda}\right)^2, \quad w(z) = w_0\left(1 + \left(\frac{\lambda z}{\pi w_0^2}\right)^2\right)^{1/2}, \quad \text{and} \quad \tan\phi_0(z) = \frac{\lambda z}{\pi w_0^2}.$$

Two Gaussian beam approximations for $k = 20, 50$ are displayed in Figure 14.

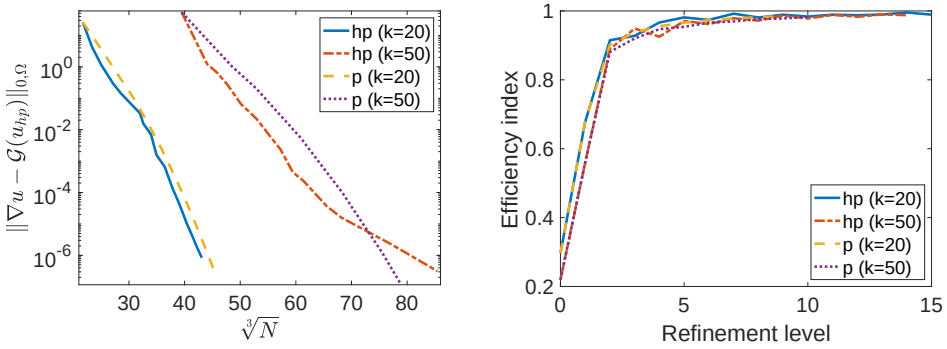

FIG. 11. *Exponential convergence (left) and efficiency indices (right) of the p- and hp-versions for the example in section* 5.3 *with* 69° *refraction.*

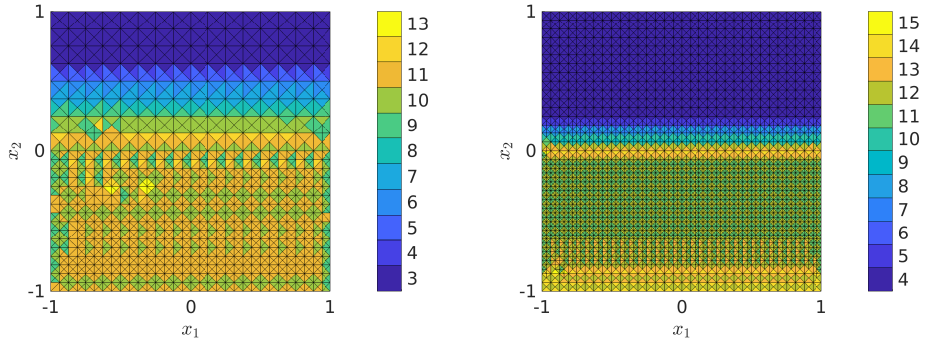

FIG. 12. *hp-refined meshes for the example in section* 5.3 *with* 29° *reflection using* $k = 20$ *(left) and* $k = 50$ *(right), where the polynomial degree is indicated with different shading.*

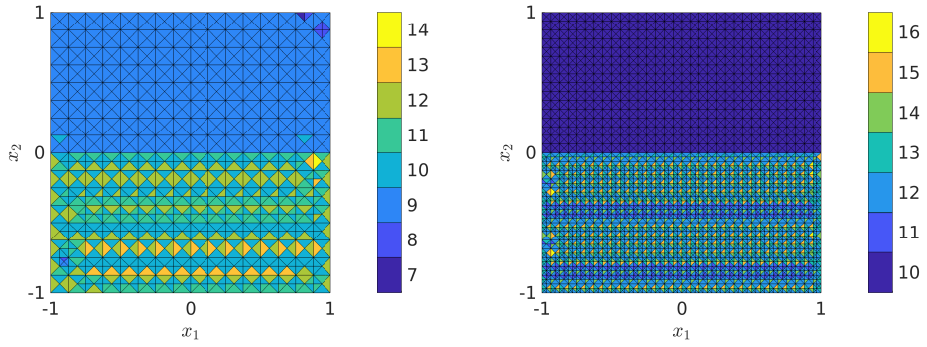

FIG. 13. *hp-refined meshes for the example in section* 5.3 *with* 69° *refraction using* $k = 20$ *(left) and* $k = 50$ *(right), where the polynomial degree is indicated with different shading.*

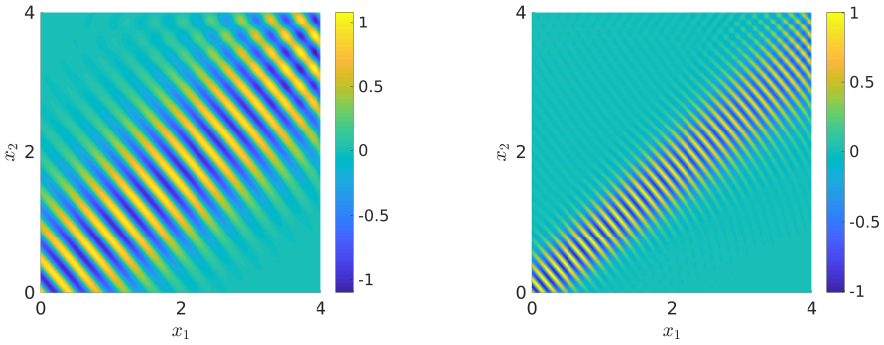

FIG. 14. *Real parts of Gaussian beam approximations for* $k = 20$ *(left) and* $k = 50$ *(right).*

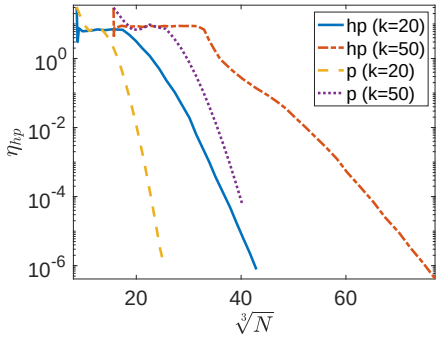

FIG. 15. *Exponential convergence of the p- and hp-versions for the Gaussian beam simulation in section* 5.4.

Since the exact solution is not known in this particular example, we only plot the values for the equilibrated a posteriori error estimator for $k = 20, 50$ in Figure 15, whose values we have demonstrated in the previous experiments should match well with those of the true error. For the initial mesh construction, we take the rather large value $C_{\text{res}} = 2$; hence, we observe a pre-asymptotic region for the convergence, which in the case of *hp*-refinement is longer than for *p*-refinement. Due to this, *hp*-refinement leads to a higher number of degrees of freedom for the same accuracy than *p*-refinement. However, both *p*- and *hp*-refinements lead to exponential convergence of the a posteriori error estimator. The two final *hp*-refined meshes are displayed in Figure 16. In particular, for $k = 50$ we observe that the polynomial degree is higher closer to the beam than further away from the beam towards the upper left and lower right corners of the domain.

6. Conclusion. We have presented an equilibrated a posteriori error estimator for the indefinite Helmholtz problem based on a nontrivial extension of the unified theory for the elliptic problem using a shifted Poisson problem. We have shown that the presented error estimator is both reliable and efficient, provided that the equilibrated flux and potential reconstructions are suitably chosen. We have provided several numerical experiments which verify that, after escaping the pollution regime, the a posteriori error estimator is efficient and reliable. In contrast to a residual-based a posteriori error estimator, we demonstrated that the presented error estimator is

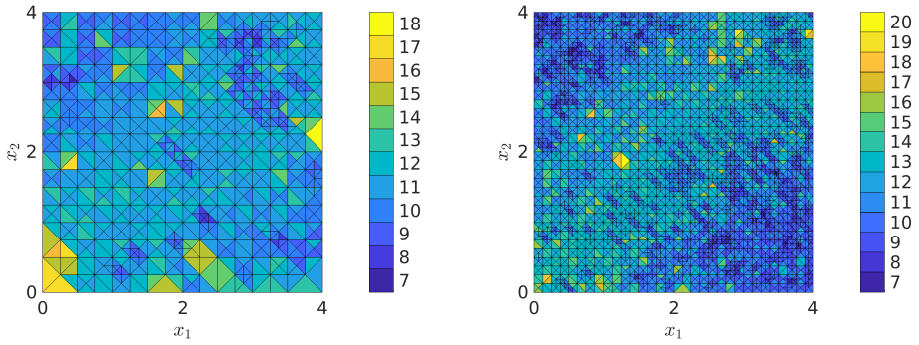

FIG. 16. *hp-refined meshes for the Gaussian beam simulation in section* 5.4 *with* $k = 20$ *(left) and* $k = 50$ *(right), where the polynomial degree is indicated with different shading.*

robust in the polynomial degree.

Note that the analysis for the potential reconstruction in section 4.2 is a purely 2D argument. A different analysis approach for the 3D case has recently been proposed in [13], together with the extension of the 2D stability result of [4]. Therefore, a potential extension of this current work would be to consider the 3D case.

Acknowledgment. The authors thank the anonymous referees for their valuable comments and suggestions that led to an improvement of the presentation of the paper.

REFERENCES

[1] I. Babuška, F. Ihlenburg, T. Strouboulis, and S. K. Gangaraj, *A posteriori error estimation for finite element solutions of Helmholtz' equation. I. The quality of local indicators and estimators*, Internat. J. Numer. Methods Engrg., 40 (1997), pp. 3443–3462.

[2] S. Beuchler, V. Pillwein, and S. Zaglmayr, *Sparsity optimized high order finite element functions for H(*div*) on simplices*, Numer. Math., 122 (2012), pp. 197–225, https://doi.org/10.1007/s00211-012-0461-0.

[3] D. Boffi, F. Brezzi, and M. Fortin, *Mixed Finite Element Methods and Applications*, Springer Ser. Comput. Math. 44, Springer, Heidelberg, 2013, https://doi.org/10.1007/978-3-642-36519-5.

[4] D. Braess, V. Pillwein, and J. Schöberl, *Equilibrated residual error estimates are p-robust*, Comput. Methods Appl. Mech. Engrg., 198 (2009), pp. 1189–1197, https://doi.org/10.1016/j.cma.2008.12.010.

[5] E. Cancès, G. Dusson, Y. Maday, B. Stamm, and M. Vohralík, *Guaranteed and robust a posteriori bounds for Laplace eigenvalues and eigenvectors: Conforming approximations*, SIAM J. Numer. Anal., 55 (2017), pp. 2228–2254, https://doi.org/10.1137/15M1038633.

[6] E. Cancès, G. Dusson, Y. Maday, B. Stamm, and M. Vohralík, *Guaranteed and robust a posteriori bounds for Laplace eigenvalues and eigenvectors: A unified framework*, Numer. Math., 140 (2018), pp. 1033–1079, https://doi.org/10.1007/s00211-018-0984-0.

[7] C. Carstensen and S. A. Funken, *Fully reliable localized error control in the FEM*, SIAM J. Sci. Comput., 21 (2000), pp. 1465–1484, https://doi.org/10.1137/S1064827597327486.

[8] C. Carstensen, J. Gedicke, and D. Rim, *Explicit error estimates for Courant, Crouzeix-Raviart and Raviart-Thomas finite element methods*, J. Comput. Math., 30 (2012), pp. 337–353, https://doi.org/10.4208/jcm.1108-m3677.

[9] O. Cessenat and B. Despres, *Application of an ultra weak variational formulation of elliptic PDEs to the two-dimensional Helmholtz problem*, SIAM J. Numer. Anal., 35 (1998), pp. 255–299, https://doi.org/10.1137/S0036142995285873.

[10] O. Cessenat and B. Després, *Using plane waves as base functions for solving time harmonic equations with the ultra weak variational formulation*, J. Comput. Acoust., 11 (2003), pp. 227–238, https://doi.org/10.1142/S0218396X03001912.

[11] V. Dolejší, A. Ern, and M. Vohralík, *hp-adaptation driven by polynomial-degree-robust*

a posteriori error estimates for elliptic problems, SIAM J. Sci. Comput., 38 (2016), pp. A3220–A3246, https://doi.org/10.1137/15M1026687.

[12] A. Ern and M. Vohralík, *Polynomial-degree-robust a posteriori estimates in a unified setting for conforming, nonconforming, discontinuous Galerkin, and mixed discretizations*, SIAM J. Numer. Anal., 53 (2015), pp. 1058–1081, https://doi.org/10.1137/130950100.

[13] A. Ern and M. Vohralík, *Stable Broken H^1 and* $\mathbf{H}(\mathrm{div})$ *Polynomial Extensions for Polynomial-Degree-Robust Potential and Flux Reconstruction in Three Space Dimensions*, preprint, https://arxiv.org/abs/1701.02161, 2017.

[14] X. Feng and H. Wu, *hp-discontinuous Galerkin methods for the Helmholtz equation with large wave number*, Math. Comp., 80 (2011), pp. 1997–2024, https://doi.org/10.1090/S0025-5718-2011-02475-0.

[15] C. J. Gittelson, R. Hiptmair, and I. Perugia, *Plane wave discontinuous Galerkin methods: Analysis of the h-version*, M2AN Math. Model. Numer. Anal., 43 (2009), pp. 297–331, https://doi.org/10.1051/m2an/2009002.

[16] S. Kapita, P. Monk, and T. Warburton, *Residual-based adaptivity and PWDG methods for the Helmholtz equation*, SIAM J. Sci. Comput., 37 (2015), pp. A1525–A1553, https://doi.org/10.1137/140967696.

[17] R. S. Laugesen and B. A. Siudeja, *Minimizing Neumann fundamental tones of triangles: An optimal Poincaré inequality*, J. Differential Equations, 249 (2010), pp. 118–135, https://doi.org/10.1016/j.jde.2010.02.020.

[18] J. M. Melenk, *On Generalized Finite-Element Methods*, ProQuest LLC, Ann Arbor, MI, 1995.

[19] J. M. Melenk, A. Parsania, and S. Sauter, *General DG-methods for highly indefinite Helmholtz problems*, J. Sci. Comput., 57 (2013), pp. 536–581, https://doi.org/10.1007/s10915-013-9726-8.

[20] J. M. Melenk and B. I. Wohlmuth, *On residual-based a posteriori error estimation in hp-FEM*, Adv. Comput. Math., 15 (2001), pp. 311–331 (2002), https://doi.org/10.1023/A:1014268310921.

[21] I. Perugia and D. Schötzau, *The hp-local discontinuous Galerkin method for low-frequency time-harmonic Maxwell equations*, Math. Comp., 72 (2003), pp. 1179–1214, https://doi.org/10.1090/S0025-5718-02-01471-0.

[22] S. Petrides and L. F. Demkowicz, *An adaptive DPG method for high frequency time-harmonic wave propagation problems*, Comput. Math. Appl., 74 (2017), pp. 1999–2017, https://doi.org/10.1016/j.camwa.2017.06.044.

[23] S. Sauter and J. Zech, *A posteriori error estimation of hp-dG finite element methods for highly indefinite Helmholtz problems*, SIAM J. Numer. Anal., 53 (2015), pp. 2414–2440, https://doi.org/10.1137/140973955.

[24] R. Verfürth, *A Review of A Posteriori Error Estimation and Adaptive Mesh-Refinement Techniques*, John Wiley & Sons, Chichester, B. G. Teubner, Stuttgart, 1996.